QUANTITATIVE MEASUREMENT OF TACKINESS

AND BONDING POTENTIAL OF TRACKLESS TACK COAT

A Dissertation

by

AH YOUNG SEO

Submitted to the Office of Graduate and Professional Studies of
Texas A&M University
in partial fulfillment of the requirements for the degree of

DOCTOR OF PHILOSOPHY

Chair of Committee,	Maryam Sakhaeifar
Committee Members,	Robert Lytton
	Amy Epps Martin
	Anastasia Muliana
Head of Department,	Robin Autenrieth

December 2019

Major Subject: Civil Engineering

ABSTRACT

Application of tack coats prior to placement of a thin overlay is a prerequisite to bond between the existing and the overlaid layers. Although a conventional tack is appropriately applied to the surface, this material is likely to be picked up and contaminated by construction traffic. Trackless tacks, recently introduced to paving industries in Texas, have overcome such issue by minimizing tackiness. However, there is no specification and documentation for tackiness and bonding potential of various trackless tacks in the Texas Department of Transportation. Also, a damage model for tackiness is needed to characterize the fracture properties of the tacks. The main objectives of this study were to 1) investigate the material characterization of trackless tacks, 2) evaluate the bonding potential of trackless tacks, and 3) develop a predictive model for the tracking behavior based on a fundamental fracture theory. Six different products were used in this study. The rheological and viscoelastic properties of trackless tacks were identified using the frequency sweep test and the multiple shear creep recovery test. The contact angle was measured to determine the surface energy characteristics. Also, the tackiness was measured at different temperatures and debonding rates using the Dynamic Shear Rheometer tackiness test and quantified in terms of tack energy. Also, the bond strength and bond energy of trackless tack coats were measured in bonded pavement layers through laboratory and field testing for evaluation of their bonding potential. The results were used to classify the trackless tack coats based on their stiffness in terms of complex shear modulus. The stiff binder group

showed to have lower sensitivity of non-recoverable creep compliance and percent recovery to stress level and better tracking resistance than the soft binder group. The curve of the tack energy varying bonding/debonding rates and temperatures could be fitted with a power law. Through a shear test, the surface type, tack type, and reactivation temperature were identified to be the dominant parameters that influence on bonding potential. Using the modified Paris's law, the fracture properties of tack residue could be obtained from the tackiness test of tack materials.

ACKNOWLEDGEMENTS

I would like to thank my committee chair, Dr. Sakhaeifar, and my committee members, Dr. Lytton, Dr. Epps Martin, and Dr. Muliana for their guidance and comments throughout the course of this research. I sincerely appreciate Dr. Arámbula of the Texas A&M Transportation Institute and Dr. Benjamin of the Department of Mechanical Engineering for their service as a substitute. I acknowledge the support from the Texas Department of Transportation, tack material suppliers, and the Texas A&M Transportation Institute. I acknowledge that the material from the dissertation is reproduced with permission of the Transportation Research Board. I thank Bryan Wilson for his assistance and feedback while being involved in the project. I also thank Ramanadham Palaniyappan and Biju Tulasi Anand for their collaborative works during the project. I thank my colleagues and department staff for giving me a good memory at Texas A&M University. Specially, thanks to my family for their encouragement and endless help to complete the course.

CONTRIBUTORS AND FUNDING SOURCES

This work was supervised by a dissertation committee consisting of Dr. Sakhaeifar, Dr. Lytton, and Dr. Epps Martin of the Department of Civil Engineering, and Dr. Muliana of the Department of Mechanical Engineering. The test devices used for this research were provided by Dr. Zhou and Bryan Wilson of the Texas A&M Transportation Institute and Dr. Little of the Department of Civil Engineering. The sample preparation of mixtures was conducted in part by Ramanadham Palaniyappan and Biju Tulasi Anand. The work of statistical analysis in Chapter 4 was performed in collaboration with Bryan Wilson. The development of analytical model in Chapter 5 was mainly guided by Dr. Lytton. All other work conducted for the dissertation was completed by the student independently.

Graduate study was supported by research and teaching assistantships from Texas A&M University. This work was also made possible in part by the Texas Department of Transportation under Grant Number FHWA/TX-16/0-6814-1. Its contents are solely the responsibility of the authors and do not necessarily represent the official views of the Texas Department of Transportation.

TABLE OF CONTENTS

Page

LIST OF FIGURES

Page

LIST OF TABLES

Page

CHAPTER I

INTRODUCTION

Background

Appropriate selection of a tack coat is essential as it governs the bonding quality of overlaid pavements (Mohammad et al. 2012, Tashman et al. 2006, West et al. 2005, Al-Qadi et al. 2008). Poor bonding may cause problems such as slippage, cracking and debonding at the interface of a flexible pavement, resulting in the rapid degradation of the pavement (Weston 2003). Although the tack is appropriately applied to the surface, the critical issue for the use of a conventional tack coat is its stickiness to vehicle tires. The material is likely to be picked up and contaminated by construction traffic. Moreover, the loss of tacks in the wheel path reduces the efficiency of a tack application and may impact on bonding between layers.

To overcome the tracking issue, trackless tacks were recently introduced to paving industries in Texas. These tacks are formulated to harden shortly after application and minimize their tackiness. However, these products are fairly new and more research on the characterization of trackless tacks needs to be done. There is no specification and documentation for tackiness and bonding potential of trackless tacks in the Texas Department of Transportation. Also, a model for predicting the tackiness is needed to consider all dominant parameters that influence the tracking issue.

Objectives

The ultimate goal of this research was to contribute to the understanding and performance evaluation of trackless tack materials. This study will achieve the following objectives:

- Fundamental research on material characterization (e.g., rheology, surface energy characteristics) of trackless tacks.
- Evaluation of tackiness involved with the adhesion of tack residues and another material and cohesion of the residues.
- Investigation of factors that influence tracking resistance.
- Comparison of bonding potential of trackless tacks to a conventional tack.
- Validation of laboratory findings with field data from test sections.
- Development of a damage model of tracking

Scope

Chapter 2 presents the literature review on material composition, tack properties and, surface energy characteristics, and bonding potential of tack coats. Chapter 3 introduces trackless tacks used in this study and the test procedures adopted for the characterization of different tack materials. Chapter 4 describes the analysis of the test results. Chapter 5 presents the detailed description of a damage model of tracking. Finally, Chapter 6 presents the conclusions and recommendations based on the findings from this study and recommends the future works.

CHAPTER II

LITERATURE REVIEWS

To understand a tack coat material and its characteristics, this study covers the literature review on the following topics:

- Composition of tack coats;
- Adhesion and surface energy;
- Tracking resistance; and
- Bonding potential.

Composition of Tack Coats

Tack coat products are manufactured in the form of a hot-applied performance grade (PG) binder or an emulsified binder. The PG binder used as a tack material is typically modified with polymers like rubber or latex for the improvement of bonding and ductility. Also, it needs lots of heat energy in order to be sprayed on the surface. The emulsified binder, on the contrary, exhibits lower viscosity than the base binder, which enables the material to be applied at low temperatures. The low temperature application reduces heat energy and provides less hazardous environment for workers so that this technique becomes cost-effective and environmentally friendly (Takamura et al. 2001). Due to these advantages, manufacturers are bringing more emulsified asphalts to the market.

A typical asphalt emulsion is composed of numerous asphalt droplets in water with emulsifier and additive (Figure 1). As asphalt and water are immiscible liquid phases, the addition of emulsifying agents and milling process is required to disperse a liquid phase in the form of droplets in the other phase (Bibette et al. 1999). The emulsifiers, also referred to as surfactants, consist of a hydrophilic group in head and a hydrophobic group in tail. The hydrophilic group of the surfactant faces water and the hydrophobic end attaches to oil. In particular, the surfactants are important chemicals to lower the interfacial tension of the liquid phase, therefore helping to prevent coalescence of the asphalt droplets in water. Since the surfactants are produced in a water-insoluble form, acid or alkali is occasionally used to formulate a water-soluble form with a charge.

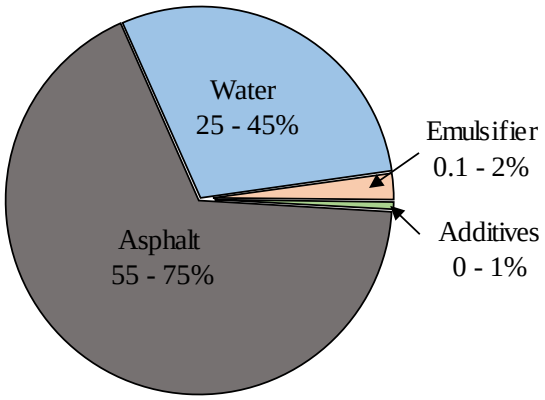

Figure 1 A typical example of emulsified asphalt composition.

Asphalt emulsions are classified based on their reactivity, physical properties, and particle charge (James 2006). The charge type on the droplets is governed by the charge on the hydrophilic group of the surfactant. The droplets in Anionic emulsions possess a negative charge, and the emulsions are known as alkaline. The Cationic

emulsions have droplets with a positive charge and are typically acid. Nonionic emulsions have no charge and are neutral in pH. Also, asphalt emulsions can be classified with respect to the setting rate: rapid-setting, medium-setting, and slow-setting. Rapid-setting emulsion is a reactive emulsion and is typically used in chip seals. Medium-setting emulsion is commonly used in open-graded mixes whereas slow-setting emulsion is an unreactive emulsion and is used as tack coat.

The reactivity of the emulsion is highly dependent on the concentration of surfactants (Boussad and Martin 1996). For instance, if surfactants are highly concentrated in the emulsion, the droplet size of emulsions will become smaller, thereby increasing the stability and elongating the setting time.

The breaking and setting rates of emulsions also depend on physical and chemical factors (Hanz et al. 2008, Bahia et al. 2008). For slow-setting emulsions, the critical factor of emulsion breaking is the loss of water, which may be influenced by climatic conditions of temperature and humidity. Another physical factor can be loading like a mechanical rolling that reduces the space between the droplets. However, the chemical reactivity between the emulsion and minerals of aggregate mostly accelerates the breaking and setting process by the change of pH level. For instance, the surface of siliceous aggregate tends to be negatively charged in the presence of water while carbonate rocks are positively charged in water. The reaction between the carbonate aggregate and cationic emulsion increases the level of pH which causes the loss of charge on the emulsions.

The emulsions undergo four transition stages until their residues are obtained, as described in Figure 2, which was modified from the work of James (2006). In the initial state, the asphalt droplets maintain separation because the charges on the asphalt droplets repel each other. However, as droplets become closer, it becomes unstable and results in adhesion (James 2006). This stage is referred to as breaking which is a quick process containing the destabilization and flocculation (Redelius and Walter 2006). Stage three is referred to as setting which is a slow process involving the coalescence of the floccules and water removal (Redelius and Walter 2006). In this process, water is drained between droplets, and droplets coalesce (James 2006). When droplets are in contact with the mineral, they bond to the aggregate surface. Stage four is a curing process when the emulsions are set after the water is completely evaporated. For this period, it is theoretically considered that the mechanical properties of emulsion residues are developed similarly to those of the base binder (Hanz et al. 2008).

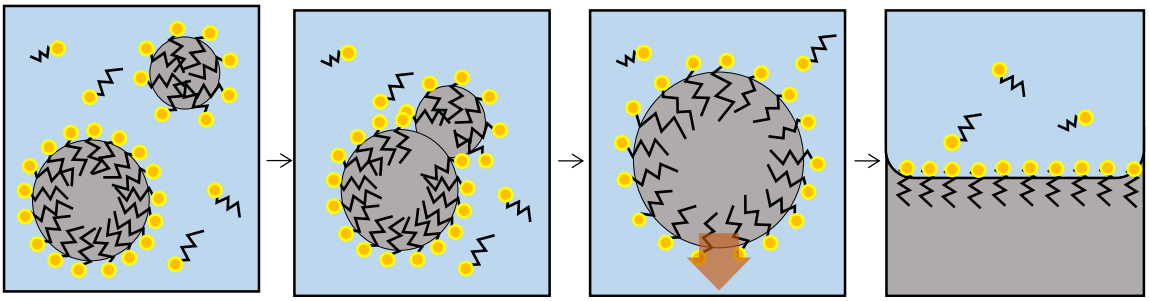

(a) stage one **(b) stage two** **(c) stage three** **(d) stage four**

Figure 2 Breaking and setting process modified from the work of James (2006).

Adhesion

Adhesion is an important physical property to determine the bonding of tack coats. The adhesion is an indication of sticking dissimilar materials and can be quantified based on the thermodynamic work of adhesion and measuring the fracture energy (Mittal 1976). Howson et al. (2012) and Okamatsu et al. (2001) investigated the relationship between the thermodynamic work of adhesion and fracture energy. While the thermodynamic work of adhesion is determined through surface energy components regardless of experimental factors, the fracture energy involves energy dissipated by plastic and viscous deformations during mechanical testing. Such difference contributes to a larger value of the fracture energy than the thermodynamic work of adhesion depending on viscoelastic properties and geometry (i.e. adhesive thickness) of the specimen. It was concluded that although two quantitative indicators of adhesion do not have the same magnitude, the thermodynamic work of adhesion is highly dependent to the fracture energy.

Factors Affecting Adhesion

Extensive research on polymeric adhesives or pressure sensitive adhesives have identified critical variables impacting the tack adhesion. These variables can be mainly divided into three categories: contact size, rheology, and surface energy.

Contact size relies on contact time and pressure, and surface roughness. When a substrate is in contact with an adhesive, a wetting surface is initially small. The adhesive bonds are enhanced with the increase in contact time (Zosel 1997, Zosel 1989). Higher

contact pressure also provides better adhesion. However, the contact time is irrelevant to adhesion under conditions where the contact force is fairly high (Grillet et al. 2012) or the adhesive behaves like a viscoelastic fluid (Schach and Creton 2008). Roughness has negative impact on adhesion between an adhesive and a substrate due to the smaller contact area on a rough surface (Zosel 1998, Grillet et al. 2012).

Rheology is also an important parameter to determine the tack adhesion (Grillet et al. 2012, Zosel 1989, Gent and Schultz 1972, Zosel 1998, Creton 2003). Dahlquist (1969) found that a pressure sensitive adhesive having an elastic modulus less than $3x10^5$ Pa at a frequency of 1 Hz and a room temperature can deform to make good contact with a substrate. This criterion has been a well-known requirement for tack performance.

As fibrils forms in a polymeric material during debonding process, the material is able to dissipate energy highly dependent on debonding rate and temperature (Zosel 1998). Grillet et al. (2012) concluded that for a material in good contact with the substrate, its adhesive force and energy exponentially increase with higher debonding rate. This is in good agreement with the result of a high-molecular weight polymer with the cohesive fracture shown in the work done by Ondarçuhu (1997). However, further increase in debonding rate lowers the bond energy and leads to the adhesive failure where an external radial crack propagates. When a fibrillar debonding is transited to a non-fibrillar debonding in the adhesive failure region, initial fracture mechanism changes from bulk yielding to crack propagation. A relaxation process is significantly

restrained at higher debonding rate, leading to no fibril formation and decrease in energy (Creton and Fabre 2002).

Surface and interfacial surface energies are dominant contributors to adhesive behaviors (Wagoner and Foegeding 2018, Zisman 1963, Song et al. 2019). Song et al. (2019) emphasized the interfacial interactions between a liquid and a solid to determine the wettability of the liquid to the substrate rather than total surface energy of each material. In an asphalt-aggregate system, many studies have successfully evaluated the moisture susceptibility of asphalt concrete based on surface energy (Howson et al. 2011, Bhasin et al. 2006, Hefer et al. 2006, Little et al. 2006, Ahmad 2011). Generally, the asphalt has high dispersive forces, and the aggregate exhibits high polarity (Khan et al. 2014). The adhesive bond of the mixture is mostly governed by the interaction between the base component of aggregate and acid components of asphalt (Bhasin et al. 2006). However, the presence of water in mixture deteriorates the adhesion between the asphalt and aggregate because the aggregate is more likely to attract water having higher polarity than the asphalt (Howson et al. 2011, Bhasin et al. 2006, Hefer et al. 2006, Ahmad 2011).

Aging has a substantial impact on the bonding of asphalt-aggregate system. Yi et al. (2018) reported that aging decreases the adhesive force and the surface energy of asphalt binders. Cheng et al. (2002) demonstrated that the aging effect decreases the polar surface energy component of the asphalt and increases the dispersive energy component. Consequently, the loss of polar interactions in the system lowers the fatigue cracking resistance. However, researchers from Western Research Institute (WRI) found

that the effect of aging on the chemical and physio-chemical properties of unaged binders is different depending on their chemistry and the severity of aging. As a result, aging can affect the different trends of the surface energy and moisture resistance of the asphalts (Robertson et al. 2001).

Besides, Majidzadeh and Herrin (1967) proved that the tensile strength of adhesive-adherend system increases as the thickness of an adhesive layer decreases. It was observed that the asphalt with thick films fails in shear. The localized rupture and fibrils form in the failure of the samples with intermediate films while brittle fracture occurs for those with thin films.

Surface Energy and Thermodynamic Work of Adhesion

Surface energy is the excess energy of molecules on the surface of a material. Molecules in the bulk of a material form cohesive forces in all directions. However, molecules at the surface do not create forces outwards the surface where they interact with air molecules (see Figure 3). Such phenomenon is induced by an imbalanced force field.

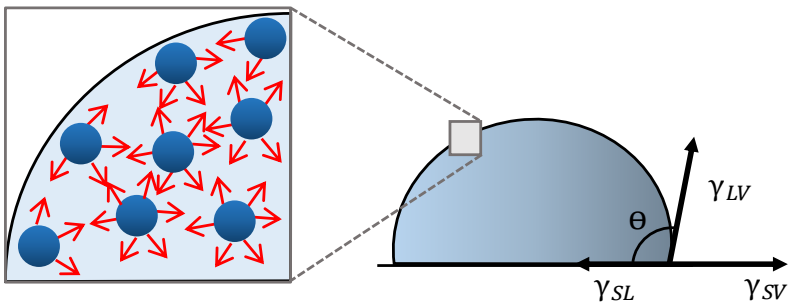

Figure 3 Surface tension in a sessile drop.

Surface energy can also be defined as the work required to increase the surface per unit area. The Gibbs free energy (G) indicates the difference between initial and final energy state of a system and is also defined as the excess energy of a system associated with surface. Thus, its change is equal to the work done on a material with a negative sign in a reversible process. The work of cohesion or adhesion (W) and the change in the Gibbs free energy are expressed in terms of surface energies (γ). The work of cohesion for a material (i) is defined as

$$W^c = -\Delta G_i^{\,c} = 2\gamma_i \tag{1}$$

When a brittle material experiences crack under loading, two new surfaces are created, and therefore the work done on the material is identical to twice the surface energy per unit surface area. In the case of different materials contacted at the interface, the work of adhesion between the materials is expressed in Dupré's equation as follows:

$$W^a = -\Delta G_{ij}^{\,a} = \gamma_i + \gamma_j - \gamma_{ij} \tag{2}$$

where, γ_i and γ_j are the surface energies of materials i and j, and γ_{ij} means the surface energy at i and j interfaces.

Consider a liquid droplet deposited on a solid with exposure to air, as shown in Figure 3. If vapor, liquid and solid are denoted by V, L, and S respectively, a force in the horizontal direction shall be balanced with regard to the corresponding interfacial energies of a thermodynamic equilibrium (Young 1805).

$$\gamma_{SV} = \gamma_{SL} + \gamma_{LV}\cos\theta \tag{3}$$

where, γ_{SV} , γ_{SL} , and γ_{LV} are the interfacial energies of solid-vapor, solid-liquid and liquid-vapor, respectively. θ is the equilibrium contact angle of a liquid droplet on solid surface. This Young's equation describes the extent of wettability based on the observed contact angle. If the contact angle is less than 90 degree, the solid surface is likely to be wetted by a liquid. Conversely, the surface is non-wetting if the contact angle is more than 90 degree.

If *i*, *j* and *ij* are denoted as liquid-vapor, solid-vapor, and liquid-solid interface, the combination of Equation (2) and Equation (3) leads to Young-Dupré's equation as follows:

$$W^a = \gamma_{LV}(1+\cos\theta) \tag{4}$$

The above equation expresses the work of adhesion between liquid and solid in terms of γ_{LV} and θ, which are easily measurable quantities through an experimental test.

The work of adhesion between liquid and solid is also described using acid-base theory. According to this theory, the surface energy components are comprised of Lifshitz-van der Waals interactions, referred to as nonpolar components, and acid-base interactions which are referred to as polar components (Van Oss et al. 1987).

$$\gamma^{tot} = \gamma^{LW} + \gamma^{AB} \tag{5}$$

where, γ^{tot} is the total surface energy of a material, γ^{LW} represents the Lifshitz-van der Waals component of the surface energy. γ^{AB} is the acid-base component of the

surface energy and equal to $2\sqrt{\gamma^+\gamma^-}$. Here, the Lewis acid components (γ^+) involve the electron acceptor interactions, and the Lewis base components (γ^-) relate to electron donor interactions. Another expression of the work of adhesion is finally obtained as:

$$W^a = 2\sqrt{\gamma_S{}^{LW}\gamma_L{}^{LW}} + 2\sqrt{\gamma_S{}^{+}\gamma_L{}^{-}} + 2\sqrt{\gamma_S{}^{-}\gamma_L{}^{+}} \quad (6)$$

The combination of Equation (4) and Equation (6) is expressed in the following equation presented by Van Oss et al. (1988):

$$\gamma_{Li}(1+\cos\theta_i) = 2\sqrt{\gamma_S{}^{LW}\gamma_{Li}{}^{LW}} + 2\sqrt{\gamma_S{}^{+}\gamma_{Li}{}^{-}} + 2\sqrt{\gamma_S{}^{-}\gamma_{Li}{}^{+}} \quad (7)$$

In order to obtain unknown surface energy components ($\gamma_S{}^{LW}$, $\gamma_S{}^{+}$, and $\gamma_S{}^{-}$) of a solid in this equation, the contact angles shall be measured using at least three different liquids with known surface energies.

Wettability is the ability of a material to wet another material and in good relation with adhesion. From a thermodynamic concept, the degree of wetting can be determined by the difference between adhesive and cohesive bond energy (Little et al. 2006). It is also be expressed as spreading coefficient, S , and calculated by the following equation:

$$S = W^a - W^c \quad (8)$$

where, W^c and W^a are the cohesive and adhesive bond energies calculated from Equation (1) and (6), respectively. If the adhesive bond energy of asphalt-aggregate combination is greater than the cohesive bond energy of asphalt, the asphalt will wet the

surface of aggregate. Also, the asphalt the higher positive value of S will show better coating on the aggregate.

Quantitative Measurement of Tackiness

Typically, a peel test (Aubrey et al. 1969) and an axisymmetric probe test (Aymonier et al. 2003, Tordjeman et al. 2000) are used to measure tack properties of adhesives. While the peel test helps obtain the complex stress near the peel region, a probe test can qualitatively identify the coupling effect of the interfacial and bulk properties on adhesion during the bonding and debonding processes (Crosby and Shull 1999).

In pavement community, several test procedures for assessing the tracking resistance of trackless tacks have been established. The no-pick-up time test was used by researchers at the Virginia Center for Transportation Innovation and Research to characterize tracking resistance (Clark et al. 2012). This test is conducted in general accordance with ASTM D 711. The stainless steel roller is fitted with rounded gaskets, and the rolling speed across the tack sample and tracking paper is controlled by allowing the device to freely roll down a ramp. The test is used to measure the level of tracking at different curing times. The results showed that the trackless materials had superior tracking resistance under room temperature and oven dried conditions to conventional material.

The roller tracking test, developed by the chemical company BASF, modified some equipment to improve the original procedure (Kadrmas 2012). This test rolls a steel wheel with rubber square-cut O-rings at predetermined curing time intervals across a tack sample applied with a wider applicator. The length of tack tracked onto a white piece of cardstock is measured. The limited research studies using these methods show

that it cannot clearly distinguish the difference between similar samples nor different temperatures. Also, a high variance can result from manual operation when this device is used.

Gorsuch et al. (2013) developed a probe test procedure by using the Dynamic Shear Rheometer (DSR) in compression and tension modes for measuring tackiness. The difference observed between tacky and non-tacky binder samples is involved with different shapes of force versus time curves. The promising advantages of the test are that the DSR device enables one to prepare samples simply and carefully control test parameters to examine various factors affecting tackiness (Gorsuch et al. 2013). Therefore, this test procedure was selected in this study to characterize the trackless tack materials with regard to tacky properties. In addition, the results of this study point out different findings from the previous research works.

Bonding Potential

Many previous studies assessed maximum bond strength by testing the laboratory or field compacted samples in shear, tension, and torque. The shear tests are widely used due to the simplicity of the test procedure and the load-displacement curve obtained that can help develop the models to characterize the behavior. The research team at the National Center for Asphalt Technology (NCAT) (Tran et al. 2012, West et al. 2005) developed the Shear NCAT Bond Strength Device. NCAT researchers suggested that the device can be used successfully to assess the bond strength and that a minimum strength of 689.5 kPa (100 psi) is recommended (West et al. 2005). This

recommendation was subsequently lowered to 551.6 kPa (80 psi). Mohammad et al. (2012) created the Louisiana Interlayer Shear Strength Tester (LISST) to determine the optimum application methods, device and calibration procedures for emulsified tack coats. The LISST was used for characterizing the interface shear strength of the laboratory and field specimens. The researchers gave a minimum bond strength recommendation of 275.8 kPa (40 psi). Other devices with a similar setup include the layer-parallel direct shear test (Raab and Partl 2008), and a shear test from the Virginia Transportation Research Council (McGhee and Clark 2009).

Unlike other studies measuring the bond strength, Hakimzadeh et al. (2012) determined a tensile fracture energy using the Interface Bond Test (IBT) to evaluate the bond between the pavement layers. It is worth mentioning that, their results based on the IBT test show that a conventional tack coat has better performance than a trackless tack coat in low temperatures, which is in contrast with the findings of few other studies such as Bae et al. (2010) and Mohammad et al. (2010) based on the shear test.

Different factors affecting the bond strength at the interface glued with tack coats have been investigated by different researchers (Al-Qadi et al. 2012, Mohammad et al. 2010, Mohammad et al. 2012, Tran et al. 2012, West et al. 2005, Zhao et al. 2017, McGhee and Clark 2009, Amelian and Kim 2017, Seo et al. 2015). The factors in most of these studies are tack coat type, surface type, mixture type, temperature, and residual tack rate. The findings of these studies are that surface roughness has a high impact on the interlayer shear strength, and surface milling provides a remarkable increase in shear strength. It was also observed that higher temperature lowers the interface shear strength,

and the effect of tack type on shear bond strength is different depending on the mixture type.

However, different observations were reported on the tack application rate. The results of the study conducted by McGhee and Clark (2009) showed no effect of tack application rate on shear strength. West et al. (2005) reported an inverse relationship between application rate and shear strength for a fine-graded mixture, while no relation was observed for a coarse-graded mixture. Amelian and Kim (2017) suggested that excessive application rate of the tack coat may have a negative impact on bonding at the interface due to the formation of a slippage plane in the lubricant layer of the tack coat. Mohammad et al. (2012) concluded that higher application rate lowers shear bond strength in laboratory compacted samples, whereas the opposite result was observed in field cores. In the study conducted by Al-Qadi et al. (2012), the optimum tack coat application rate was recommended depending on surface type, tack coat type, and cleanliness. Zhao et al. (2017) reported that the tack application rate and mixture type are less important factors that influence the interlayer shear strength, as compared to the surface texture on cement concrete slab, tack type, temperature, and humidity.

With respect to the performance of trackless tacks, most studies (Chen et al. 2012, Clark et al. 2012, Mohammad et al. 2012, McGhee and Clark 2009) proved that trackless tacks provide higher shear strength than conventional tack coats. McGhee and Clark (2009), on the contrary, showed that the bond strength of conventional tack coats in both shear and tensile modes is higher than that of trackless tack material, albeit in a

limited test scope. Chen et al. (2012) also found that a top-down cracking resistance decreases with increasing brittleness of trackless tacks.

CHAPTER III

EXPERIMENTAL PLANS*

Material Description

Material type in each layer of asphalt mixtures is presented in Table 1. The hot mix asphalt (HMA) overlay and substrate layer are composed of Type C and D mixtures, respectively, which are widely used in Texas for resurfacing the existing pavements. Type C mixture has a coarse surface with 19-mm nominal maximum aggregate size (NMAS), whereas Type D mixture has a fine surface with 12.5-mm NMAS. The gradation of two mixtures meets the TxDOT specification indicated in Figure 4. The selected asphalt binder and the theoretical maximum specific gravity are PG 76-22 and 2.391 for the upper layer, and PG 64-22 and 2.422 for the lower layer, respectively.

Table 1 Material types used in mixture layers.

Layer	Material type
Overlay	Thin overlay mixture (TOM) type C
Substrate	Superpave mixture type D
Tack coat	1 control tack (CSS-1H) and 6 trackless tacks[a] (NTQS-1HH, NTSS-1HH, CQS-1HT, QS-1HH, CBC-1H, polymer-modified binder)

Note: [a] Trackless tack labels are randomly assigned into Tack A to E for anonymity.

* Part of this chapter is reprinted with permission from "Evaluating Tack Properties of Trackless Tack Coats Through Dynamic Shear Rheometer" by Seo, A.Y., Sakhaeifar, M.S. and Wilson, B.T. (2017) Transportation Research Record: Journal of the Transportation Research Board, 2632(1), 119–129, Copyright 2017 by National Academy of Sciences and "Performance Evaluation and Specification of Trackless Tack" by Wilson, B. T., Seo, A. and Sakhaeifar, M. S. (2016) College Station, TX: Texas A&M Transportation Institute, FHWA/TX-16/0-6814-1, Copyright 2016 by Texas A&M Transportation Institute.

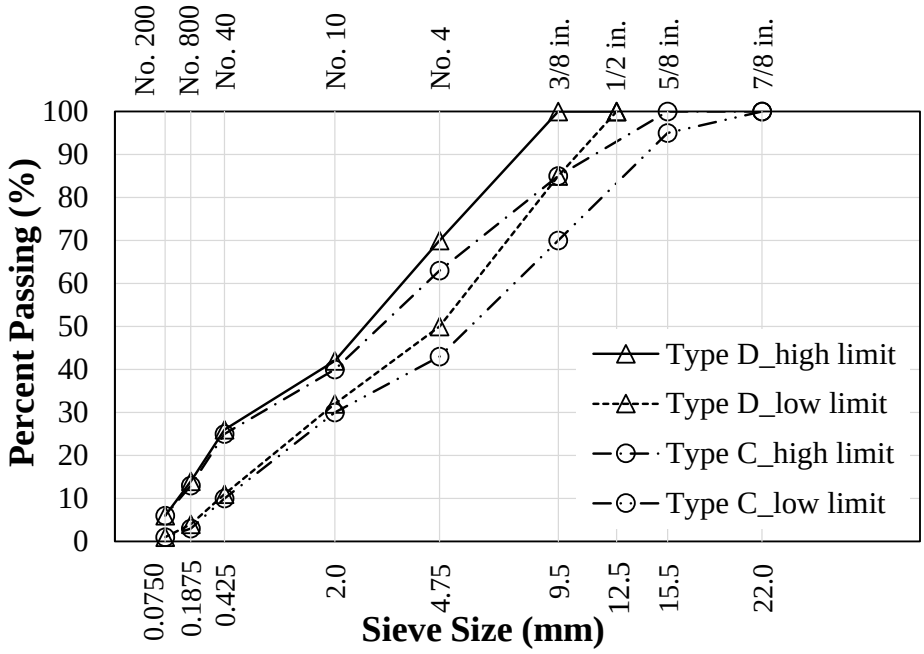

Figure 4 TxDOT specifications for type C and D mixtures.

Tack coat materials used in this study include one conventional tack and six different trackless tacks. The researchers of this study contacted several asphalt emulsion suppliers and requested samples of the tack materials from various manufacturers. The control tack, CSS-1H, is a traditional cationic emulsion that consists of a hard asphalt with slow-setting and low viscosity. The trackless tacks include two cationic emulsified binders (CQS-1HT and CBC-1H), three anionic emulsions (NTSS-1HH, NTQS-1HH and QS-1HH), and a polymer-modified binder and are randomly labelled into Tack A to F for anonymity.

The tack emulsions were cured using the modified 6-hr evaporative method which is specified in AASHTO PP72 Method B developed by TXDOT. The low-temperature evaporation method was selected since the length of curing time is shorter

compared to previous methods. Also, a cured sample using this technique is a good representative of the one exposed to field conditions (Kadrmas 2014). The emulsion was stirred to provide a uniform dispersion of droplets and poured over a silicon mat. Then, a thin film applicator was used to obtain a thickness of 0.38 mm (0.015 in), as shown in Figure 5(a). The film thickness was measured with a wet film thickness gauge and put in an oven. The emulsion sample was cured at 60ºC for 6 hours, as presented in Figure 5(b). Then, the cured tack residue was carefully peeled off from the mat before being cooled.

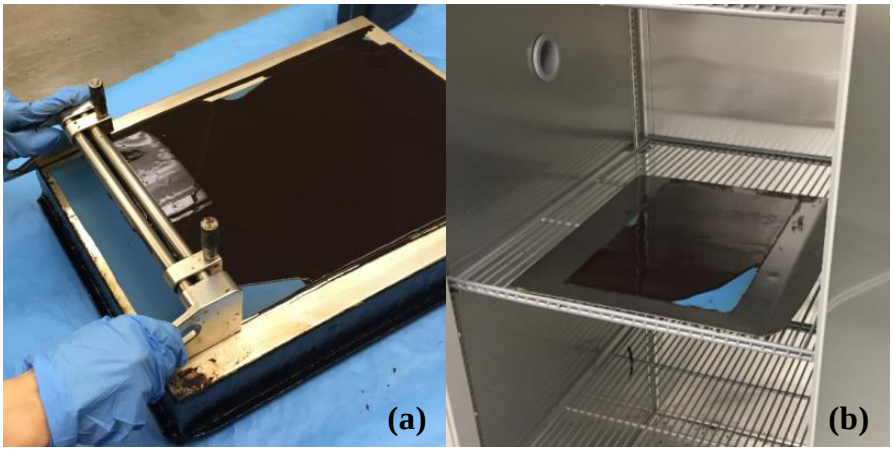

Figure 5 Sample preparation for emulsion recovery: (a) thin-film application and (b) evaporation of water in an oven.

Characterization Methods

Different properties of the tack emulsions and residues were collected as summarized in Table 2. The viscoelastic properties of tack samples were measured through different tests. The frequency sweep test and Multiple-Stress Creep-Recovery (MSCR) test were used to characterize the rheological properties of residual binders. The

contact angles of residual binders were measured to calculate the surface energy of the tack residue. The tackiness test was conducted on both tack emulsion and residue at different testing conditions. The interlayer shear resistance in terms of strength and energy was evaluated for laboratory compacted and field samples using a direct shear test. Two replicate samples of asphalt binders and three replicates of mixtures were tested. More detailed description for each test method is provided in the following section.

Table 2 Properties of tack materials and adopted test procedure in this study.

Material Type		Property	Test Procedures
Asphalt	Residue	Complex shear modulus ($\|G^*\|$) Phase angle (δ)	Frequency sweep test: AASHTO T 315
	Residue	Percent recovery Non-recoverable creep (J_{nr})	MSCR test: ASTM (D7405)
	Residue	Surface energy (γ)	Sessile drop method
	Residue/ Emulsion	Force vs. time Tack energy (G_T)	DSR tackiness test
Mixture	Lab compacted/ Field samples	Shear bond strength Shear bond energy	Direct shear test

DSR Frequency Sweep Test

The frequency sweep test was conducted to identify the undamaged rheological properties of asphalt binder by applying constant loading with low amplitude. The test was conducted over a wide range of loading frequencies at multiple temperatures using the dynamic shear rheometer. In this test, two main parameters of the asphalt binder were measured: the absolute value of the complex shear modulus, $|G^*|$, and the phase angle, δ. Here, $|G^*|$ is calculated as the ratio of maximum shear stress to maximum shear strain, indicating the resistance to deformation. The phase lag, δ, between the applied stress and responsive strain, describes the viscoelastic behavior of the tested asphalt samples.

Emulsion residues, cured through AASHTO PP72 Method B, were tested as well. The range of loading frequencies varies from 1 to 100 rad/s. The test temperature was stabilized in a forced air chamber. The 25-mm parallel plates with a 1.0 mm gap were used at high temperatures, and the 8-mm parallel plates with a 2.0 mm gap were used at intermediate temperatures.

A master curve was constructed based on a time-temperature superposition concept and the assumption of thermorheologically simple materials (Marasteanu and Anderson 2000). The desired master curve forms a single curve for the complex shear modulus versus reduced frequency. This curve is created such that the computed frequency at the reference temperature equals the loading frequency of the test condition (Clyne and Marasteanu 2004). The reduced frequency can be expressed as follows:

$$f_r = f \times a_T\left(T_i\right) \tag{9}$$

where, a_T is the shift factor as a function of the testing temperature, T_i. f is the loading frequency at the testing temperature of interest, and f_r is the reduced frequency at the loading frequency and temperature of interest. Here, the shift factor forms a second-order polynomial relationship in terms of temperature. This relationship is shown in Equation (10):

$$\log a_T\left(T_i\right) = aT_i^2 + bT_i + c \tag{10}$$

where, a, b, and c are the coefficients of the second-order polynomial function.

The master curve mathematical formulation adopted in this study is based on the Christensen-Anderson-Marasteanu model (Marasteanu and Anderson 1999). The CAM model is introduced in the following equation:

$$\left|G^*\left(\omega\right)\right| = G_g\left[1+\left(\frac{\omega_c}{\omega}\right)^{\nu}\right]^{-\frac{w}{\nu}} \tag{11}$$

where, $\left|G^*\left(\omega\right)\right|$ is the dynamic shear modulus at an angular frequency ω, and ω_c, w, and ν are the fitting coefficients. G_g is the glassy modulus, and its value is typically 1 GPa. This parameter indicates the limiting stiffness obtained at very low temperatures and high frequencies where the physical hardening of viscoelastic materials is dominant. Three shift factor coefficients in Equation (10) and three model parameters in Equation (11) were simultaneously determined using the Solver tool in Microsoft

Excel. The model parameters fitted to the data can be used to predict the value of complex shear modulus or phase angle at any desired temperature and frequency of loading within the range of testing conditions. The reference temperature considered for all master curves was 20 °C.

Multiple-Stress Creep-Recovery Test

The Multiple-Stress Creep-Recovery (MSCR) test was conducted to identify the viscoelastic properties of an asphalt binder. The MSCR test is the latest method to improve the current PG specification. This method is suggested to replace the existing dynamic shear test because of a better correlation with field performance, particularly rutting (Anderson 2011). The MSCR test has been used to investigate the effect of modification on rutting performance (Hanz et al. 2009). Furthermore, the MSCR recovery can also indicate the fatigue resistance of asphalt binder when evaluating the elastic response (Zhou et al. 2012, Mogawer et al. 2011). The test was conducted at 60°C, which is the same temperature used in the residue recovery method. At this high temperature, the 8-mm plate geometry with a 1-mm gap setting was used in the DSR.

Figure 6 shows the stress input and the strain output of a sample, as specified in ASTM D7405. In this test, the one-second creep load is applied to the sample, which causes an increase in strain. The MSCR test procedure involves two sets. A low stress level of 0.1 kPa is applied for 10 cycles in the first set, and a high stress level of 3.2 kPa is loaded for 10 cycles in the next set. After each loading cycle, the load is removed and the sample is allowed to recover for 9 seconds. The strain is partially recovered during

the unloading period and the rest remains as non-recoverable strain. As the loading cycles increase at different stress levels, the non-recoverable strain is accumulated, representing the potential of permanent deformation in pavement.

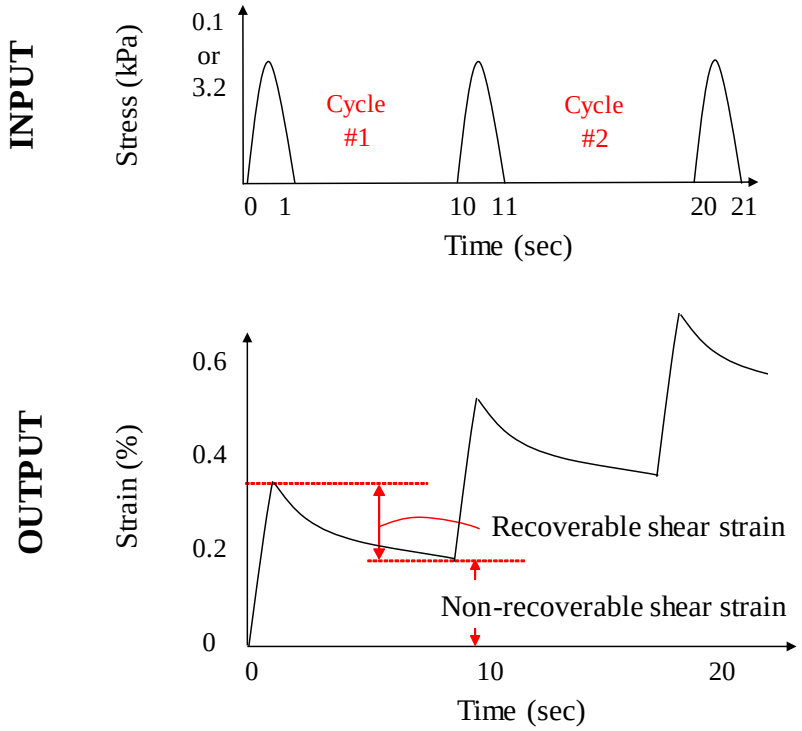

Figure 6 Input and output of MSCR test.

The parameters determined by the MSCR test are the average percent recovery and the non-recoverable creep compliance. The percent recovery is defined as the delayed elastic response of a binder and calculated through the following equation:

$$\%\text{Recovery} = \frac{\gamma_r}{\gamma_p} \times 100 \tag{12}$$

where, γ_r is the recoverable shear strain, and γ_p is the peak shear strain.

The non-recoverable creep compliance (J_{nr}) represents the residual strain after repeated loading with respect to the stress level. J_{nr} is a parameter representing the resistance to permanent deformation under repeated loading. The non-recoverable creep compliance is determined using Equation (13):

$$J_{nr} = \frac{\gamma_u}{\tau_{Applied}} \tag{13}$$

where, γ_u is the non-recoverable shear strain. $\tau_{Applied}$ is the applied shear stress.

The average percent recovery and the non-recoverable creep compliance were measured to assess if the elastic response of the binders correlates with adhesion in this study.

Sessile Drop Method

The measurement of surface tension using a contact angle has been widely used due to simplicity (Sharma and Rao 2002). A variety of testing methods have been developed to identify the surface characteristic of liquid and solid. These methods include the Wilhelmy plate, sessile drop, tilted plate, pendent drop, and capillary rise tests.

One of the widely used methods, the Wilhelmy plate method, is an indirect technique used to measure a contact angle of a solid by detecting the change of force during immersion and emersion of a solid on liquid. During a submersion cycle of a thin plate into liquid vertically, the wetting force and buoyant force contribute to the force

change in balance. It is known that this method provides a reliable result with high accuracy in measuring contact angles and contact angle hysteresis (Yuan and Lee 2013). However, it was found in this study that it is difficult to produce a rough surface of coated tack residue along a vertical line. Furthermore, sample preparation was challenging since some of the tack residues became hardened quickly while coating thin glass slides with them since the glass slides were easily broken.

The sessile drop method is known as a static contact angle method. Simply, an optical device captures the image of droplets and measures the angle between the baseline and tangent line of the droplet at an interface. The drop shall be placed on the surface falling as little as possible to minimize kinetic energy (Woodward 1999). Although there is an uncertainty of assigning a tangent line and a base line when measuring the angles due to roughness (Yuan and Lee 2013), the preparation of solid surfaces in this method is easier as compared to the Wilhelmy plate method. Also, only a small amount of a probe liquid is needed in this test. Therefore, this study used the sessile drop method for measuring contact angles of tack residues.

As the first step of the sample preparation process, the glass slides were cleaned with acetone and then rinsed with water. The glass slides were put into the oven to remove the moisture. A small quantity of asphalt was applied onto the glass slides taken from the oven. The glass slides were placed on a laboratory hotplate to provide a uniform layer of the asphalt. Finally, the samples were stored in a desiccator overnight at 20°C to remove moisture from their surface.

Appropriate selection of liquid probes is critical to correlate the measured contact angles with surface energetics of a solid (Kwok and Neumann 1999). The existence of probe liquids with similar magnitudes of surface energy can lead to high sensitivity to errors in contact angles. Therefore, diiodomethane (methylene iodide) shall be replaced with glycerol or formamide in order to minimize the error (Hefer et al. 2006). Therefore, three liquids shown in Table 3 were chosen in this study. The distilled water exhibits stronger polar surface components whereas the diiodomethane is composed of pure non-polar surface energies and has high density. The glycerol has extremely high dynamic viscosity compared to other probe liquids.

Table 3 Material property and surface energy of probe liquids.

Probe liquid	Density (kg/m^3)	Dynamic Viscosity (NS/m^2)	γ^{LW} (mJ/m^2)	γ^{+} (mJ/m^2)	γ^{-} (mJ/m^2)	γ^{AB} (mJ/m^2)	γ^{tot} (mJ/m^2)
Distilled Water	998	0.0010	21.8	25.5	25.5	51.0	72.8
Glycerol	1261	1.4120	34	3.92	57.4	30.0	64.0
Diiodomethane	3320	0.0028	50.8	0	0	0.0	50.8

***Note*:** γ^{LW} is the Lifshitz-van der Waals component of the surface energy.

γ^{+} is the Lewis acid components of the surface energy.

γ^{-} is the Lewis base components of the surface energy.

γ^{AB} is the acid-base component of the surface energy $\left(=2\sqrt{\gamma^{+}\gamma^{-}}\right)$.

γ^{tot} is the total surface energy $\left(=\gamma^{LW}+\gamma^{AB}\right)$.

Figure 7 presents the contact angle of a liquid droplet on a substrate. The contact angle is obtained from a tangent line at the border line of droplet and bottom line. By comparing the measured diameter of a needle with the estimated one, the device can estimate the dimension of droplet such as diameter, height and volume. The instrument used in this study contains no pump program so the volume of deposited droplets is controlled manually. The volume of the droplets shall be small to eliminate the gravitational effect for diiodomethane having a high density. Therefore, the pendent drops with a volume ranging from 1 to 1.5 μL were deposited on solid surface to minimize the sample to sample variance. The contact angles were measured for 60 seconds to observe their changes over time, and four measurements of contact angles on each binder sample were recorded.

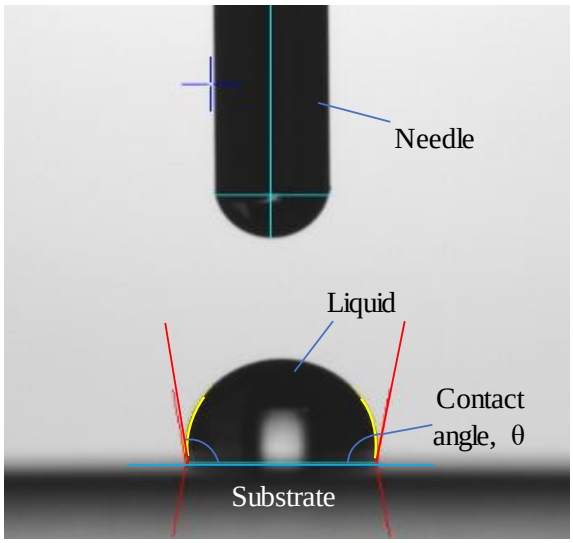

Figure 7 Contact angle measurement in the sessile drop test.

The surface energy components (${\gamma_S}^{LW}$, ${\gamma_S}^{+}$, and ${\gamma_S}^{-}$) of a solid substrate were calculated by solving the following matrix, as shown in Equation (14):

$$\begin{bmatrix} \sqrt{{\gamma_{L1}}^{LW}} & \sqrt{{\gamma_{L1}}^{-}} & \sqrt{{\gamma_{L1}}^{+}} \\ \sqrt{{\gamma_{L2}}^{LW}} & \sqrt{{\gamma_{L2}}^{-}} & \sqrt{{\gamma_{L2}}^{+}} \\ \sqrt{{\gamma_{L3}}^{LW}} & \sqrt{{\gamma_{L3}}^{-}} & \sqrt{{\gamma_{L3}}^{+}} \end{bmatrix} \begin{bmatrix} \sqrt{{\gamma_S}^{LW}} \\ \sqrt{{\gamma_S}^{+}} \\ \sqrt{{\gamma_S}^{-}} \end{bmatrix} = \frac{1}{2} \begin{bmatrix} {\gamma_{L1}}^{tot}(1+\cos\theta_1) \\ {\gamma_{L2}}^{tot}(1+\cos\theta_2) \\ {\gamma_{L3}}^{tot}(1+\cos\theta_3) \end{bmatrix} + \mathbf{e} \qquad (14)$$

where, **e** is the error matrix. Using the Excel solver by iteration, the sum of squares of errors in the matrix shall be minimized to determine the surface energy components of the solid. The standard deviations of the surface energy components of the solids were calculated by error propagation. Detailed illustration is given in the study conducted by Little et al. (2006). Once the surface energy components of tack residues were obtained, the adhesive and cohesive bond energies of the tacks in contact with different materials were calculated using Equation (1) and (6). The wettability of the tacks on the substrate surface was estimated using Equation (8).

The materials considered as an adherend in this study are vehicle tire, stainless steel, and aggregate. The surface energy components of the stainless steel were obtained from this study using the DSR plate made of 316L stainless steel. For the surface energy of tires and aggregates, typical materials that the previous studies examined were selected in this study, as shown in Table 4. The surface energy of rubber materials were identified using a sessile drop test method in the work of Al-Assi and Kassem (2017). The surface energy components of various aggregate types were measured using the Universal Sorption Device (USD) in the study of Little et al. (2006).

Two rubber materials have a low total surface energy, and their main surface energy component is the dispersive component. There exist a low magnitude of base components and no acid components for the rubber materials. In particular, Styrene Butadiene Rubber (SBR) has higher dispersive and lower base parts of surface energy than nitrile. On the contrary, the total surface energy of aggregate widely ranges from 48 to 356 mJ/m^2 depending on aggregate type and is much higher than rubber. This result is due to various magnitude of polar surface energy components. Gravel has the highest dispersive and polar surface energy components. Limestone shows the lowest base component, and granite has the lowest acid component of surface energy.

Table 4 Surface energy of different adherends: (a) rubber and (b) aggregate.

Substrate	γ^{LW} (mJ/m^2)	γ^{+} (mJ/m^2)	γ^{-} (mJ/m^2)	γ^{AB} (mJ/m^2)	γ^{tot} (mJ/m^2)
(a) Rubber*					
Styrene Butadiene Rubber (SBR)	22.11	0	2.24	0	22.11
Nitrile	17.08	0	10.33	0	17.08
(b) Aggregate**					
Limestone	44.1	2.37	259	49.5	93.6
Gravel	57.5	23	973	299.3	356.8
Granite	48.8	0	412	0	48.8

***Note*:** * Results of Al-Assi and Kassem (2017)

** Results of Little et al. (2006)

DSR Tackiness Test

The DSR machine was also utilized in the second round of tests to characterize the tack properties of different sample types. The test procedures are based on the work done by Gorsuch et al. (2013) who used similar equipment to assess the base and residual binders. This study involves two sets of testing. The first set is for emulsion testing and the second one is for residue testing. The emulsion samples were tested throughout the curing period.

The samples were tested using a Kinexus Rotational Rheometer manufactured by Malvern. For measuring the tackiness of emulsions, tack samples were applied at a uniform thickness of 0.38 mm on a strip of asphalt paper using a wet film applicator. This piece of paper was then cut into 2-cm by 2-cm squares and placed in the oven at the specified curing temperature. At the specified curing time, the paper coated with tacks was removed from the oven and fixed on a plate using high-strength double-sided tape, as shown in Figure 8(a).

In residue testing, the tack residue was poured on a 25-mm DSR mold and cooled in a refrigerator. After cooling, the residue was pressed to achieve 1 mm-thickness with a caliper, and the sample was placed on the 25mm DSR bottom plate, as shown in Figure 8(b).

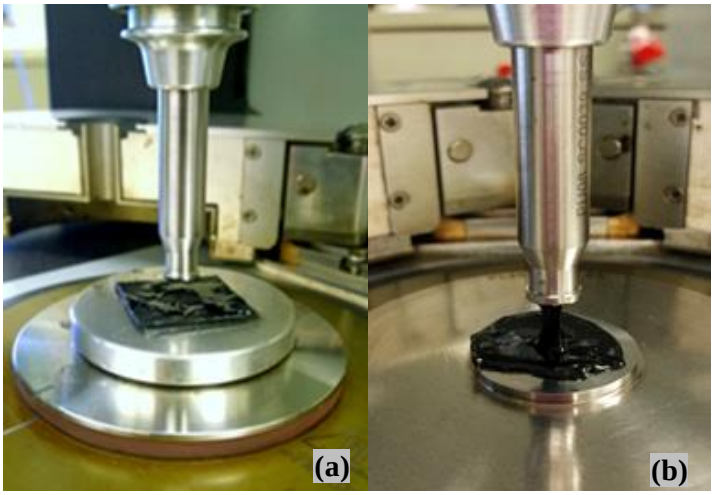

Figure 8 DSR tackiness test using (a) emulsion and (b) residue samples.

The samples on both sets of testing were preheated over 60°C for 5 to 10 minutes to remove the remaining moisture from its surface and prevent possible debonding at the interface between the sample and bottom plate. The samples were loaded with an 8-mm DSR tip. The temperature chamber was stabilized at target temperatures in 5 minutes, and then the sample was loaded at 10.5 N for 10 seconds. After 10 seconds of loading, the tip was lifted off the sample up to 10 mm. The loading and debonding rates are 1.0 mm/sec, typically. The load-time plot was recorded throughout the process.

The area under the load-time curve, shown in Figure 9, was used to determine tack energy which is the released energy of a tack sample until failure. The fracture energy per unit area of an interface during bond separation yields Equation (15) and was introduced by Gent and Kinloch (1971) and Andrews and Kinloch (1973).

$$G_T = \frac{r}{A}\int F(t)dt = d_t\int \sigma d\varepsilon \qquad (15)$$

where, σ and ε are the stress and the strain. F is the normal force, A is the contact area, r is the pull-off speed rate, t is time(sec), d_t is the sample thickness, and G_T indicates the tack energy. In this study, the tack energy involves the cohesive and adhesive fracture energy that is determined by weaker bonds between the cohesion of a tack sample and adhesion at the tack-DSR tip interface. The tack energy, used as an indicator to quantify the stickiness, was successfully applied for a tack measurement in previous studies (Aymonier et al. 2003, Seo et al. 2016, Zosel 1989).

Figure 9 also presents an actual representative picture of failure state at each testing condition. The failure mode is determined by observing the contaminated area on the DSR tip. The failure mode provides critical information implying the relative difference between cohesion and adhesion of the tack samples.

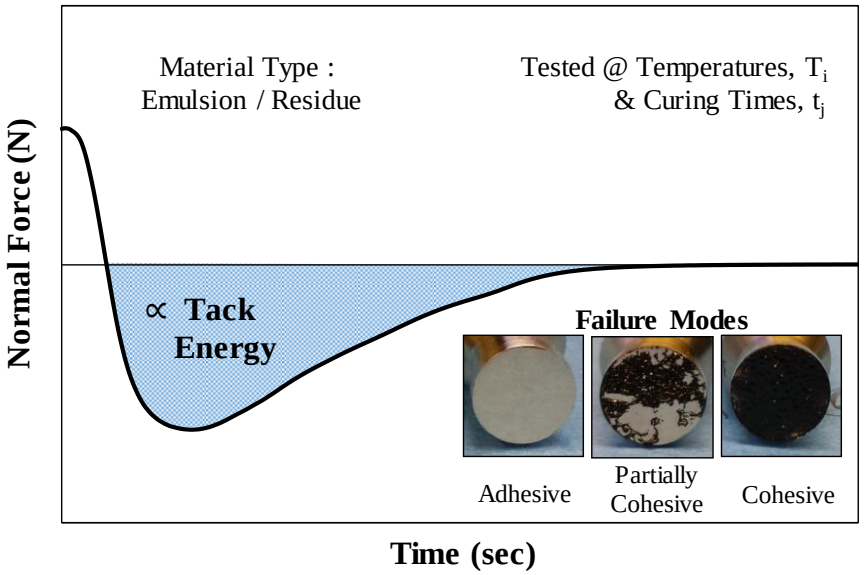

Figure 9 Estimation of tack energy from DSR tackiness test.

A clean failure surface, where a totally metallic surface is exposed, is an indication of adhesive failure at the tip. In this case, the intermolecular forces and the covalent bonds between the hydrocarbons chains in the sample are strong (Sperling 2005). As a consequence, the adhesive energy is weaker than the cohesive energy and will govern the bond failure at the interface between the tip and tack sample. In this case, the tested sample is considered to be "*trackless*".

A test with a dirty tip indicates the cohesive failure within the tack. In this case, the weak polar interactions are easily broken by external loads like heat-produced loading (Sperling 2005), and the adhesion is stronger than the cohesive bonds. The partially cohesive failure possibly occurs, and the size of the contaminated area may affect the change in tackiness.

The positive force was considered as the compression mode, and the negative force was considered as the tension mode. Although the actual contact area changed over time after the peak load, the contact area was assumed to be constant due to the lack of appropriate technique to monitor the changes. The average of two readings was used for this investigation.

Shear Bonding Test

Testing Plan

A series of dominant factors on shear bonding were evaluated. The testing plan for interlayer shear resistance is presented in Table 5. The laboratory test plan consists of small-scale experiments that consider tack type, substrate type, compaction effort, and

tack reactivation temperature of overlay and substrate layers. The samples with tack materials as well as no tack treatment were tested to identify the effect of tack type on shear bonding at the interface. To investigate the effect of substrate type on shear bonds, three substrates including severely polished HMA, mildly polished HMA and Portland cement concrete (PCC) were used. The severely polished HMA substrate was conditioned with coarse (80-grit) and fine (220-grit) sandpapers attached to an orbital sander whereas the mildly polished substrate was treated only with coarse grit sandpaper in the laboratory. Also, the compaction angle of 1 and 1.25° was chosen to determine the impact of compaction effort on interlayer shear resistance. To evaluate the effect of tack reactivation temperature, the substrates with cured tack were conditioned at 15, 25, and 40°C, and the overlay mixtures were compacted at 135 and 149°C.

Table 5 Test factorial for interlayer shear resistance.

Sample	Variable[a]	Content	Level
Laboratory compacted samples	Tack	No tack, Control tack, Tack A, Tack B, Tack C, Tack D, Tack E	7
	Substrate	Severely polished HMA, Mildly polished HMA, Portland cement concrete	3
	Tack reactivation temperature (°C)	135, 149 (Overlay)	2
		15, 25, 40 (Substrate)	3
	Compaction angle (°)	1, 1.25	2
Field cores	Tack	Tack B, Tack D	2
	Surface condition	Existing, New, Milled	3
	Residual tack rate	Low[b] (0.05-0.14 L/m^2), Moderate (0.14-0.23 L/m^2), High (0.23-0.32 L/m^2)	3

Note: [a] Some variables are not fully evaluated in the test factorial.

[b] Low rate is omitted in the milled section.

The field testing plan examines the effect of surface condition, tack type, and residual tack rate on shear bonds. The effect of surface condition was assessed through a thin overlay construction project on US 183 in Cedar Park, between Osage Drive and FM 1431. This site involves three test sections: existing HMA, new HMA, and milled sections. The existing HMA surface was significantly polished by climate and traffic exposure over the years, as shown in Figure 10(a). The pavement in most parts of the milled section was uniformly milled [Figure 10(b)]; however inconsistent milling was found in some areas of this section [Figure 10(c)].

Two trackless tacks (Tack B and D) were used in the field. Three application rates used are 0.18, 0.32 and 0.45 L/m^2 (0.04, 0.07 and 0.1 gal/yd^2), in addition to no tack application rate. The residual tack rates were measured as specified in ASTM D2995. In several sections, the residual rates were estimated on the basis of measurements from similar sections. The approximate values of residual tack rates are 0.05 to 0.14 L/m^2 (0.01 to 0.03 gal/yd^2) in low level, 0.14 to 0.23 L/m^2 (0.03 to 0.05 gal/yd^2) in moderate level, and 0.23 to 0.32 L/m^2 (0.05 to 0.07 gal/yd^2) in high level. It should be noted that the low tack application rate was omitted on the milled surface for all tacks used in the project. This was done since the low tack rate could not fully cover the surface due to high roughness in the milled sections. Three replicates for each variable were used in the laboratory and field testing plan, but the field samples with poorly milled surface shown after testing were excluded in the data analysis to minimize the impact of milling quality.

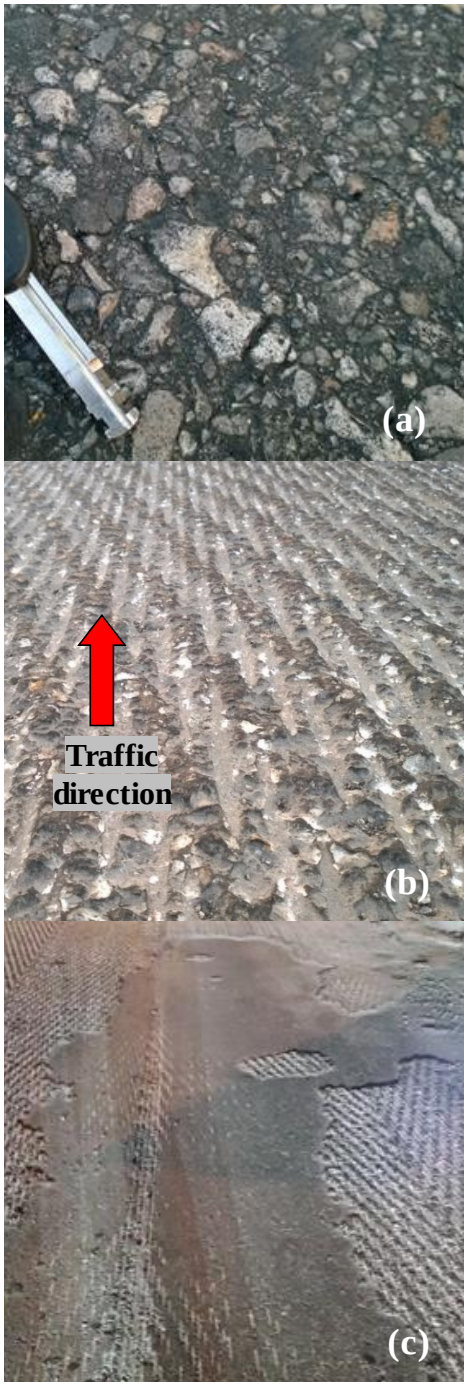

Figure 10 Surface conditions of US 183 field project including: (a) existing, (b) uniformly milled, and (c) scabbed milled surfaces.

Sample Preparation

Laboratory compacted samples were prepared with the Superpave gyratory compactor (SGC). A 150 mm (6 in) diameter substrate was compacted with 60 gyrations, to a height of approximately 51 mm (2 in). In most cases, the substrate surface was artificially aged (polished) using an orbital sander with coarse (80-grit) and fine (220-grit) sandpaper, and subsequently cleaned with an ultrasonic water bath. "New" samples were conditioned with coarse grit paper and then cleaned. Once the substrates ere dried, the heated tack was applied to the substrate with a brush at a "moderate" rate recommended by the vendor. This rate is between 0.18 and 0.27 L/m^2 (0.04 and 0.06 gal/sy) for emulsions, and 0.54 L/m^2 (0.12 gal/sy) for hot-applied tack. The samples were set to cure for 30 to 60 minutes at 60ºC and then allowed to stabilize at the specified substrate temperature. The samples were reinserted into the mold, and the overlay mix was compacted with 25 gyrations. For each sample configuration, three replicate samples were prepared. After 8 to 16 days of curing in room temperature curing, the samples were stabilized at 25°C until a direct shear test is ready.

The field samples were cored in the center of the desired lane, not along the wheel path, to eliminate the tracking effect of field results. The direction of traffic was marked on all samples in the milled section so that loads were applied at the laboratory in the same direction as marked. The samples were allowed to be fully dried before testing.

Test Procedure

The direct shear test was performed using the PINE interface shear strength apparatus presented in Figure 11. The sample was inserted with the bond interface oriented vertically. One side of the apparatus holds the specimen rigidly while the other side is free to slide vertically. A load was applied to the free-sliding side at a rate of 5 mm/min (0.2 in/min) until failure.

Figure 11 Test apparatus of direct shear test.

In this study, both shear bond strength and energy were measured to evaluate the interlayer shear resistance. The research conducted by Amelian and Kim (2017) confirmed that the energy term can be an important indicator of fatigue resistance in the shear mode. It was indicated that shear energy until a peak load has a higher correlation with the results of the cyclic shear test than shear strength. In this study, hence, the shear bond strength was determined from the peak load, and the shear bond energy was calculated to be the area under the load-displacement curve up to the peak load per unit

initial cross-sectional area of the samples. The failure location was recorded to identify if a failure mainly occurs at interface or within adjacent layers.

Lastly, an analysis of variance (ANOVA) was performed to address the sensitivity of different variables to the bonding potential. The *p*-value of 0.05 was chosen for the ANOVA test to distinguish the statistical significance.

CHAPTER IV

RESULTS AND DISCUSSION[†]

Rheological Properties

DSR Frequency Sweep Test Results

Figure 12 shows the master curves of stiffness and phase angle for different tack materials. As frequency decreased, the difference in stiffness among the materials became more significant. The control tack was the softest and most viscous of all the materials, followed by Tack A and B. The residues of Tack A and B exhibited similar stiffness values throughout a wide frequency range. Tack C belongs to the middle-ranked group with respect to its stiffness and has similar viscosity to Tack A and B at low frequency or high temperatures. Tack D, E, and F contain the hardened binders. Tack F exhibited the same rheological properties as Tack D, and the slopes of the Tack D and F stiffness curves seemed to be slightly flatter than the slope of Tack E. However, in phase angle master curves, the difference between Tack D/Tack F and Tack E was significant. Tack E was more viscous at low and intermediate frequencies than other stiff materials. It should be noted that three stiff residues did not exhibit a reverse slope in phase angle master curves at the low frequency range.

[†] Part of this chapter is reprinted with permission from "Evaluating Tack Properties of Trackless Tack Coats Through Dynamic Shear Rheometer" by Seo, A.Y., Sakhaeifar, M.S. and Wilson, B.T. (2017) Transportation Research Record: Journal of the Transportation Research Board, 2632(1), 119–129, Copyright 2017 by National Academy of Sciences and "Performance Evaluation and Specification of Trackless Tack" by Wilson, B. T., Seo, A. and Sakhaeifar, M. S. (2016) College Station, TX: Texas A&M Transportation Institute, FHWA/TX-16/0-6814-1, Copyright 2016 by Texas A&M Transportation Institute.

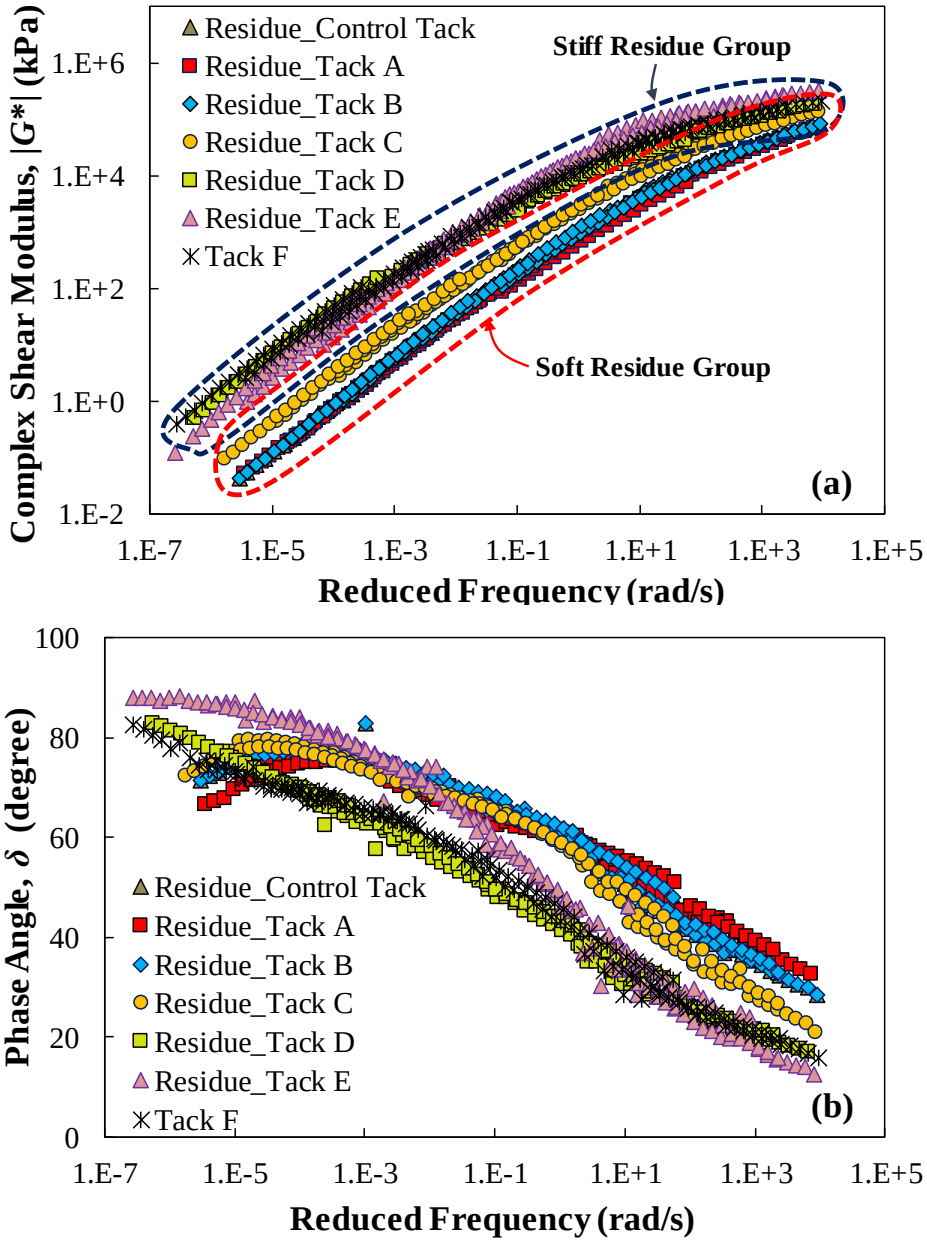

Figure 12 Mastercurves of (a) complex shear modulus and (b) phase angle for all tack coat materials.

MSCR Test Results

The average percent recovery represents the amount of recovery in strain after the unloading process. A high percent recovery represents a higher level of elasticity contribution, thereby resulting in better performance against rutting and fatigue cracking (Mogawer et al. 2011).

Figure 13 presents the percent recovery at different stress levels. The percent recovery decreased with an increase in stress level. The control tack exhibited the lowest level of recovery; this material had no recovery at the high stress level. For the soft-residue group (control tack and Tack A, B, and C), a considerable change in percent recovery was observed at higher stress condition, indicating that the residues in the soft-residue group had high sensitivity to stress level. On the contrary, the percent recovery of the stiff-residue group did not decrease significantly at higher stress levels.

Figure 14 shows the non-recoverable creep compliance of the residues of the soft- and stiff-residue groups at different stress levels. The J_{nr} increased with stress level while different tack types had a different sensitivity to stress level. The J_{nr} of the stiff-residue group was significantly lower than that of the soft-residue group. Also, the stiff-residue group was less sensitive to stress level than the soft-residue group in terms of J_{nr}. Among the stiff residues, Tack D had the lowest value of J_{nr} followed by Tacks F and E. The control tack exhibited the highest J_{nr} at two stress levels, followed by Tacks A, B, and C.

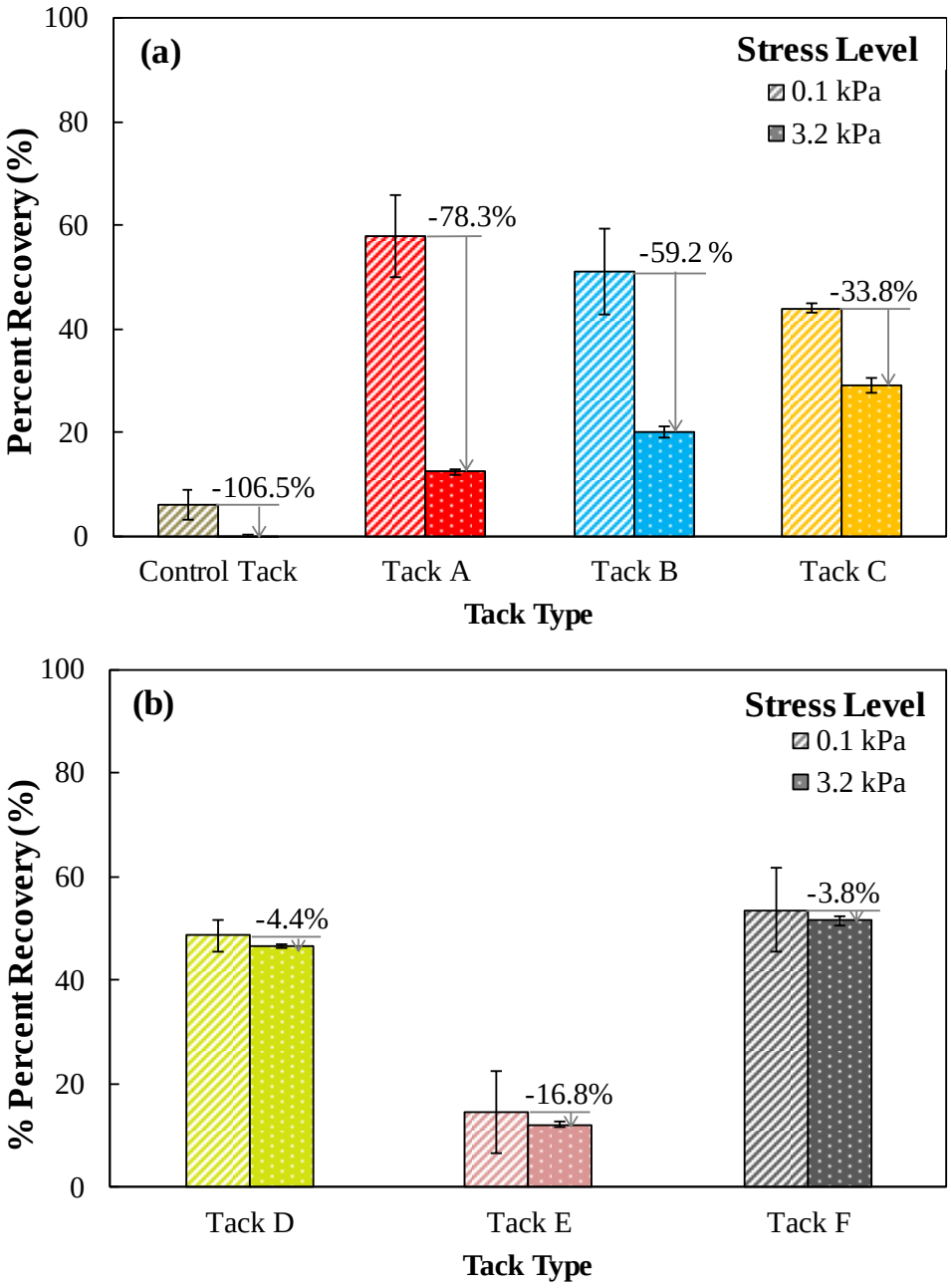

Figure 13 Percent recovery of emulsion residues: (a) soft residue group and (b) stiff residue group.

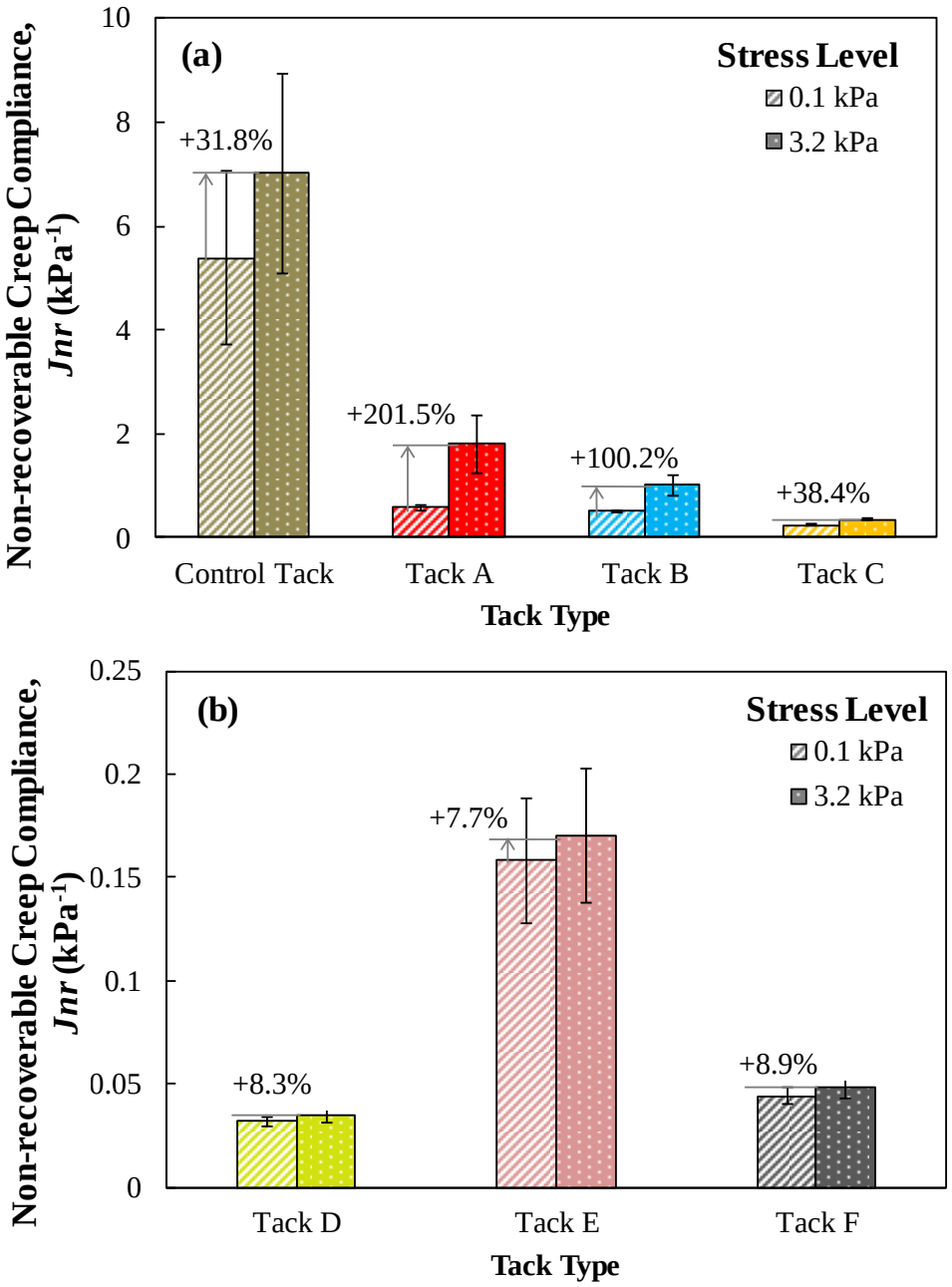

Figure 14 Non-recoverable creep compliance of emulsion residues: (a) soft-residue group and (b) stiff-residue group.

Surface Energy Characteristics

Sessile Drop Test Results

The contact angles of three tack coats (control tack, Tack C, and Tack E) and the DSR plate used in this study were measured to determine their surface energy components. Figure 15 shows the test results of three probe liquids on Tack E residue up to 60 seconds. It was seen that the contact angle and the sessile volume of water slightly decreased over time, but its base line was constant. It means that the evaporation of water into air contributed to a very small reduction in contact angle.

For glycerol, the contact angle significantly decreased at a short time, and then were stabilized. After being stabilized, the glycerol showed a constant sessile volume and base line. Since the liquid has high dynamic viscosity, 2 to 5 seconds were required to let the droplet reach to equilibrium state. Conversely, diiodomethane exhibited a continuous and significant reduction in contact angle. A gradual increase in base line indicates that the droplet of diiodomethane continued wetting the tack residue over time due to a physical or chemical reaction.

The results of probe liquids on the DSR plate are shown in Figure 16. Unlike the tack residue, diiodomethane exhibited a constant contact angle over time, indicating that no chemical or physical reaction occurs between the solvent and solid. For glycerol, about 10-40 seconds were needed to make the contact angle and base line stabilized. Water evaporation was also seen on the plate, resulting in a slight decrease in the contact angle of a water droplet.

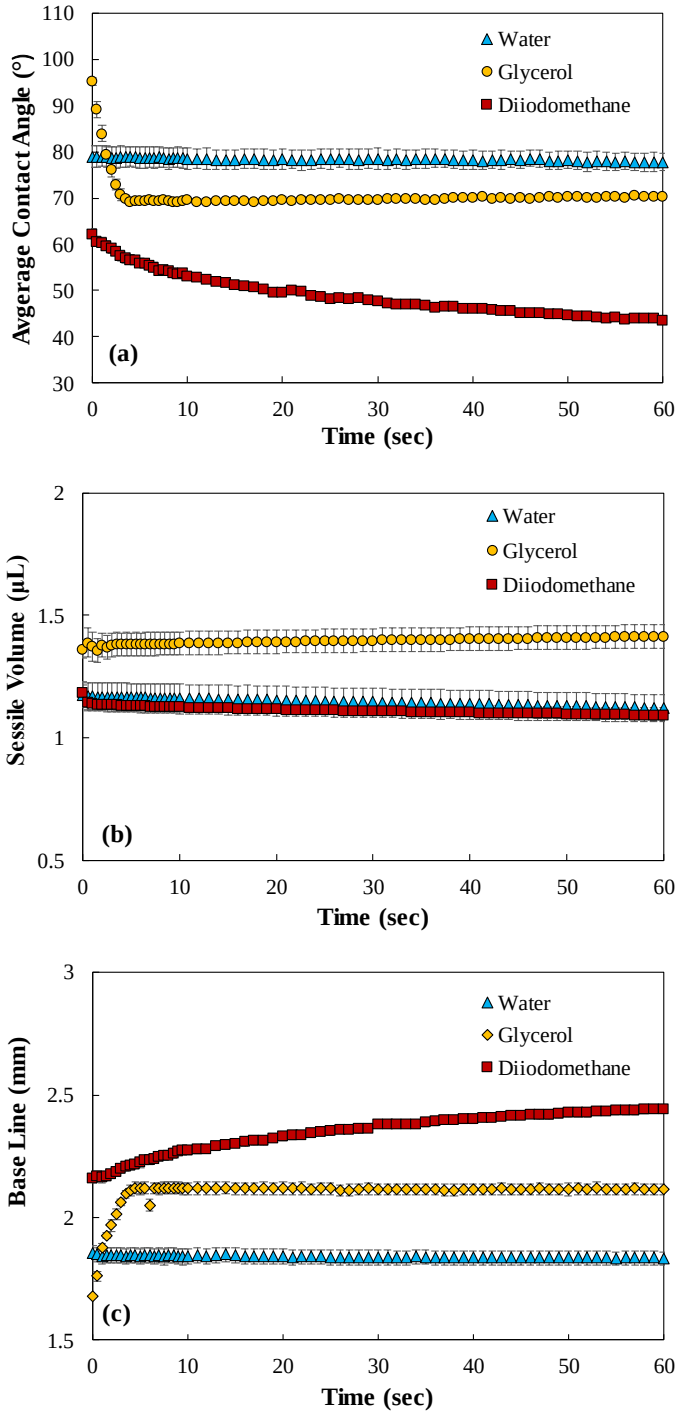

Figure 15 Results of liquid droplets on tack residues: (a) contact angle, (b) sessile volume, and (c) base line.

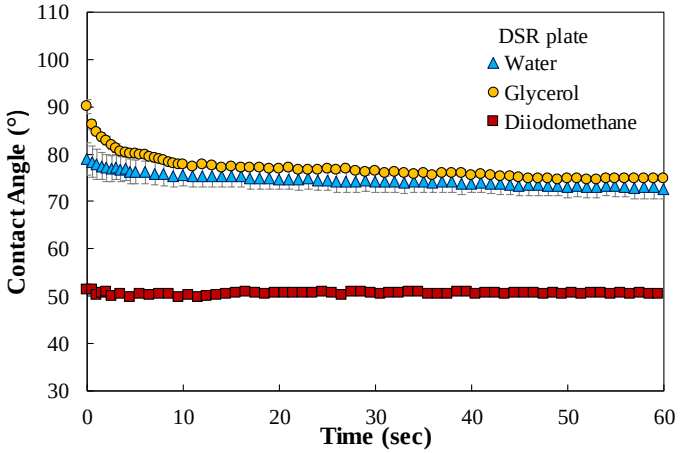

Figure 16 Contact angles of liquid droplets on DSR plate.

Kwok and Neumann (1999) stated that the apparent contact angles observed experimentally can be used to be inserted in Young's equation under the following assumptions; 1) a solid surface is smooth, and homogeneous, 2) no chemical and physical reaction between the liquid and the solid occurs so that the contact angle should be in equilibrium, and 3) the liquid has higher surface tensions than solid. A fitting curve between $\gamma_L \cos\theta$ versus γ_L measurements is recommended to check if probe liquids are suitable for applying Young's equation.

In order to determine a contact angle of each liquid applicable in Young's equation, the initial contact angle of water was chosen to eliminate the effect of evaporation on contact angle. For glycerol with high viscosity, the contact angle at 60 seconds was selected to stabilize the drop shape. Although diiodomethane dissolves asphalt, at least one non-polar solvent is required to calculate the polar components of solids. Hence, the initial contact angle for diiodomethane was selected in this study. The selected contact angles of probe liquids on different substrates are presented in Table 6.

Among the liquids, the contact angles of water for all substrates were the highest, followed by glycerol, and then diiodomethane. Since there exist some variation of the contact angles with four measurements, the validation process was conducted to identify if the average value of contact angles is suitable to meet the theoretical requirement.

Table 6 Selected contact angles of probe liquids on different substrates.

Material	Statistics	Water[a]	Glycerol[b]	Diiodomethane[a]
Control tack	AVG[c]	98.11	95.93	68.52
	STD[d]	3.26	3.43	8.74
Tack C	AVG	84.21	77.32	70.17
	STD	6.65	3.76	6.39
Tack E	AVG	78.93	70.34	62.23
	STD	4.68	1.20	2.15
Stainless steel (DSR plate)	AVG	79.03	74.80	51.77
	STD	8.58	0.50	1.19

Note: [a] Initial contact angle was selected as an equilibrium contact angle.

[b] The contact angle at 60 sec was selected as an equilibrium contact angle.

[c] Average

[d] Standard deviation

Figure 17 shows the fitting curve of $\gamma_L \cos\theta$ versus γ_L using the selected contact angles of probe liquids on the substrates. The fitting curve with a higher R-squared value implies the valid selection of the contact angles. The R-squared values of control tack, Tack C and E, and DSR plate are 0.92, 0.9, 0.83, and 0.94, respectively.

These contact angles were validated and used to calculate the surface energy components of each material.

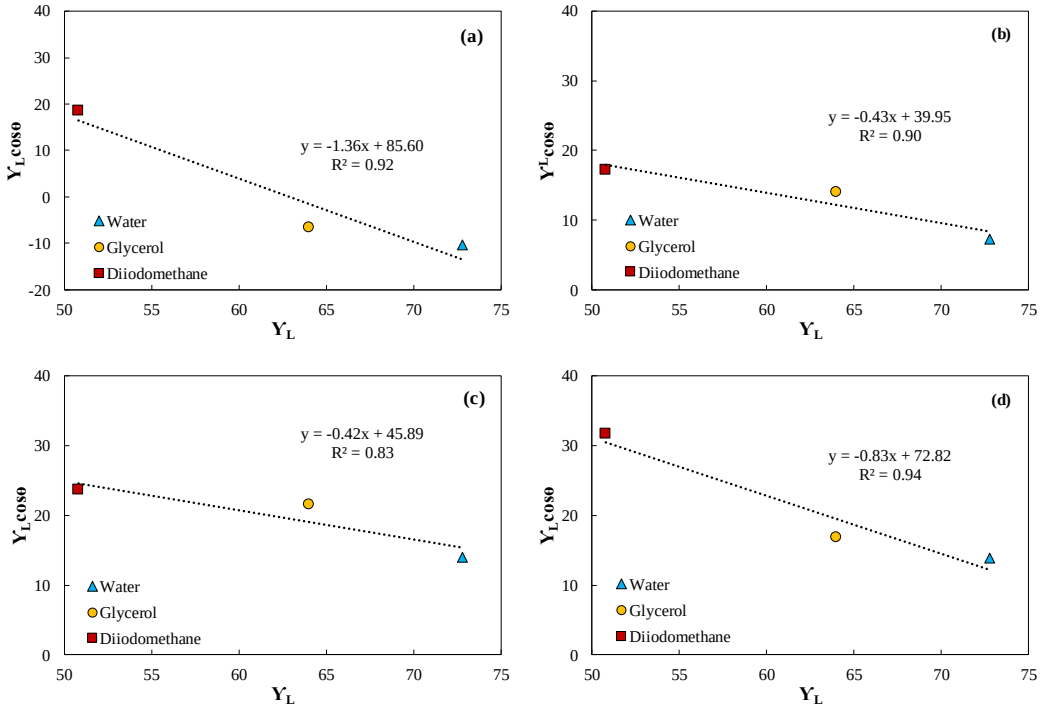

Figure 17 Validation of contact angles of probe liquids on different materials: (a) control tack, (b) Tack C, (c) Tack E, and DSR plate.

Calculation of Surface Energy

Table 7 displays the surface energies of different solids calculated by using Equation (14). The major contribution of total surface energy of the solids is the Lifshitz-van der Waals (LW) components. The acid component is the smallest, followed by the base component. Among the tack samples, Tack E shows the highest LW, acid, and base components. The total surface energies of control tack and Tack C are similar. As compared to tack residues, the stainless steel exhibits a lower acid component but higher LW and base components. The surface energy components of the stainless steel are close to the result of Boxler et al. (2014), showing a total surface energy of 43 mJ/m^2, but different from the result of Hallab et al. (2001), presenting a dispersive

component of 33.4 mJ/m^2 and a polar components of 96.24 mJ/m^2. The difference occurs because the change in roughness by surface treatment strongly affects the associated adhesion (Bueno 2005).

Table 7 Calculated surface energies of solids using contact angle.

Material	Statistics	γ^{LW} (mJ/m^2)	γ^{+} (mJ/m^2)	γ^{-} (mJ/m^2)	γ^{AB} (mJ/m^2)	γ^{tot} (mJ/m^2)
Control tack	AVG	23.70	0.30	4.98	2.43	26.13
	STD	2.46	0.28	1.47	1.21	2.75
Tack C	AVG	22.78	0.57	7.66	4.18	26.96
	STD	1.79	0.41	3.29	1.75	2.50
Tack E	AVG	27.29	0.75	8.38	5.02	32.32
	STD	0.63	0.22	2.29	1.00	1.18
Stainless steel (DSR plate)	AVG	33.44	0.002	10.15	0.31	33.75
	STD	0.35	0.015	3.73	1.00	1.05

Adhesive and Cohesive Bond Energy Based on Surface Energy

Adhesive and cohesive bond energies (W^a and W^c) based on surface energy represent the thermodynamic work of adhesion and cohesion. The bond energies of tack residues in contact with stainless steel, rubber tire, and aggregate are given in Table 8. The W^a of the tack on the rubber tire was the lowest, followed by the stainless steel and lastly the aggregate. While no difference in W^a between the control tack and Tack C was observed for the stainless steel and the rubber, the aggregate showed the big difference between two tacks. Among tacks, Tack E having high dispersive and polar surface energy components exhibited the highest adhesive and cohesive bond energies.

Table 8 Adhesive and cohesive bond energies of tack residues in different systems.

Tack	W^c	W^a (SS)	W^a (SBR)	W^a (NT)	W^a (LS)	W^a (GV)	W^a (GN)
Control tack	52.3	60.0	47.4	43.7	89.0	129.1	90.1
Tack C	53.9	60.3	47.1	44.3	96.2	146.0	97.3
Tack E	64.6	66.2	51.7	48.8	106.2	161.1	108.2

Note: Measurements in mJ/m^2

W^a is the adhesive bond energy; W^c is the cohesive bond energy.

SS = stainless steel; SBR = styrene butadiene rubber; NT = nitrile;

LS = limestone; GV = gravel; GN = granite

Using these bond energies, the wettability of the tack residues on the surface of different materials was evaluated. The wettability is quantified by the spreading coefficient S as the difference between W^a and W^c. For instance, if W^a is greater than W^c or S is positive, a material in contact with another material is a higher tendency to fail within the material. As presented in Table 9, Styrene Butadiene Rubber (SBR) and nitrile in the rubber group exhibited a negative S while the stainless steel and aggregate had a positive S. This result indicates that the tack-tire system was more likely to fail at the interface whereas the tack-stainless steel and aggregate systems had a higher occurrence of failure within the tacks. Among the tacks, the control tack showed better wettability on the stainless steel and the rubber than the trackless tacks. On the other hand, the adhesion of the control tack was inferior to that of the trackless tacks.

Table 9 Wettability of tack residues on different materials.

Tack	*S* (SS)	*S* (SBR)	*S* (NT)	*S* (LS)	*S* (GV)	*S* (GN)
Control tack	7.7	-4.8	-8.5	36.8	76.9	37.8
Tack C	6.4	-6.8	-9.6	42.3	92.1	43.4
Tack E	1.6	-12.9	-15.9	41.6	96.5	43.6

Note: *S* is the spreading coefficient (wettability) in mJ/m^2.
SS = stainless steel; SBR = styrene butadiene rubber; NT = nitrile;
LS = limestone; GV = gravel; GN = granite

DSR Tackiness Test Results

Tackiness of Tack Emulsion

Figure 18 shows the results of the DSR tackiness test on Tack A sample. There is no peak force observed in the tension mode during an initial curing time at 25°C. This happened due to incomplete evaporation of water in the emulsion sample, as seen in the tip surface at 10-minute curing time. However, the peak force and area under force curves increased while the sample was cured. At the curing temperature of 40°C, the tack samples reached to a stickier state after 20-minutes of curing time, showing a constant magnitude of the peak forces and area under force curves over times. The samples at the temperature of 60°C became liquid-like and showed cohesive failure mode. It is worth mentioning that the testing condition of 60°C led to an asymptote value for tack strength at different curing times. The contamination on the tip surface with low tack strength was not a desirable result for the trackless tack.

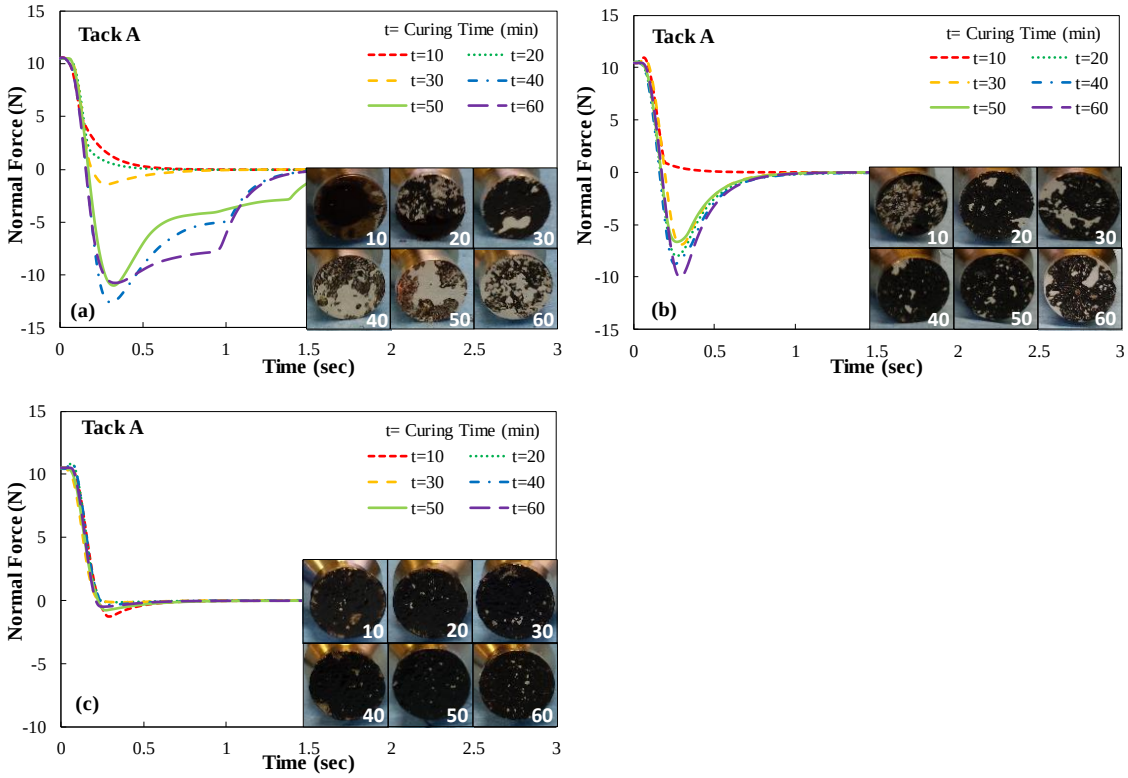

Figure 18 Force versus time curve for Tack A emulsion cured at different temperatures: (a) 25°C, (b) 40°C, and (c) 60°C.

Figure 19 presents the DSR tackiness test results of Tack E. Over curing times at the room temperature, there was no interaction between the DSR tip and sample, which indicates that the tackiness did not exist at all. Even when the curing temperature was increased to 40°C, the tackiness properties of the sample did not significantly change with curing time and the force curve did not reach to tension mode zone. However, the temperature of 60°C resulted in considerable stickiness with contamination of the tip at different curing times. In addition, the peak force at a high temperature of Tack E was greater than that of Tack A, meaning that Tack E was sticker than Tack A.

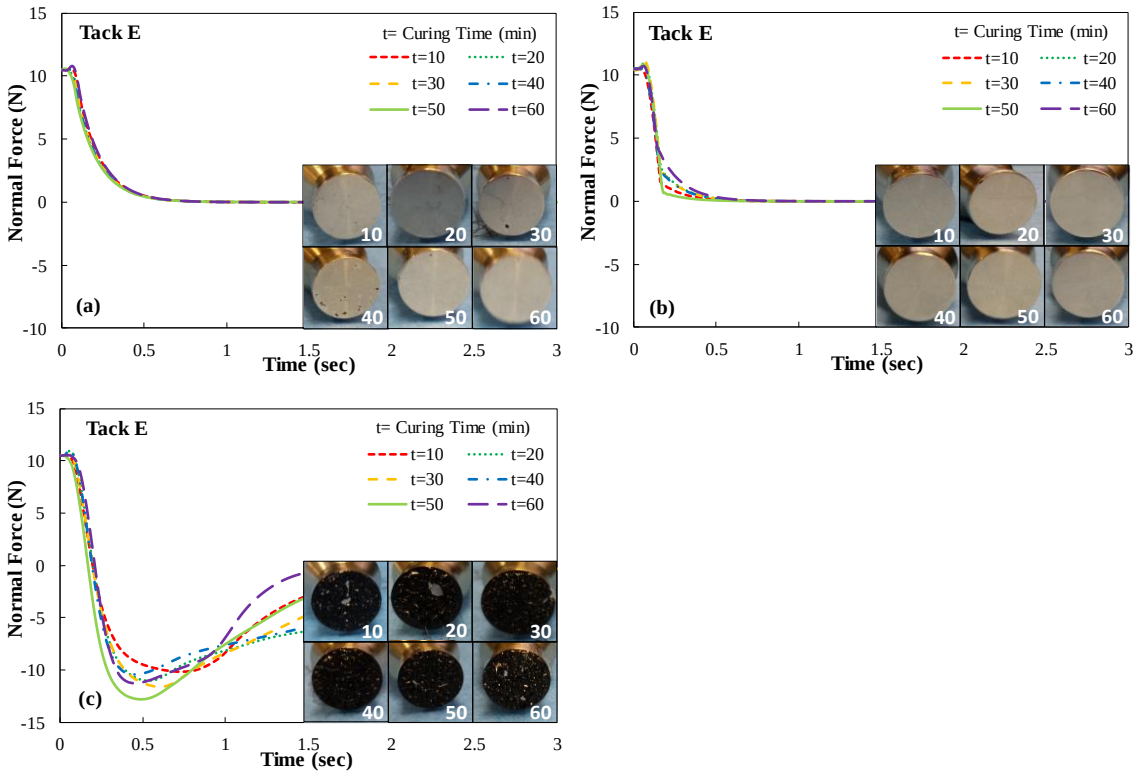

Figure 19 Force versus time curve for Tack E emulsion at different temperatures: (a) 25°C, (b) 40°C, and (c) 60°C.

The tack energy for all the tacks at different levels of curing is presented in Figure 20 where a clear distinction was observed between the soft (Control tack, Tack A, B, and C) and stiff binder group (Tack D, E, and F) with respect to tack energy. At 25ºC, the tack energy of all tack materials except the control tack and Tack A was close to zero, and adhesive failure occurred during different curing times. Since the solid-like tack sample possessed strong cohesive strength, the interface failure was dominant. In the tests at 40ºC, the stiff binder group (Tack D and E) also exhibited low tack energy and failed at the interface. The tack energy of Tack B at 40ºC led to a combination of adhesive and cohesive failure modes. This failure mode led to a high sensitivity in

response depending on the degree of wetting of Tack B to the tip surface. At 60ºC, all tacks were softened and completely governed by cohesive failure, resulting in a consistent tack energy with curing times. While the tack energy of the soft binder group was low, the stiff binder group exhibited the highest tack energy. It was observed that the soft binder group became more liquid-like, but the stiff one was close to a sticky rubber under this condition. The control tack at 25ºC, Tack C at 40ºC after 20 minutes and Tack F at 60ºC exhibited that the cohesive strength of the sample or the adhesive strength between the tip and sample surface exceeded the strength of other supporting elements. From these results, it can be concluded that the value of tack energy in such condition is challenging to measure using the current method.

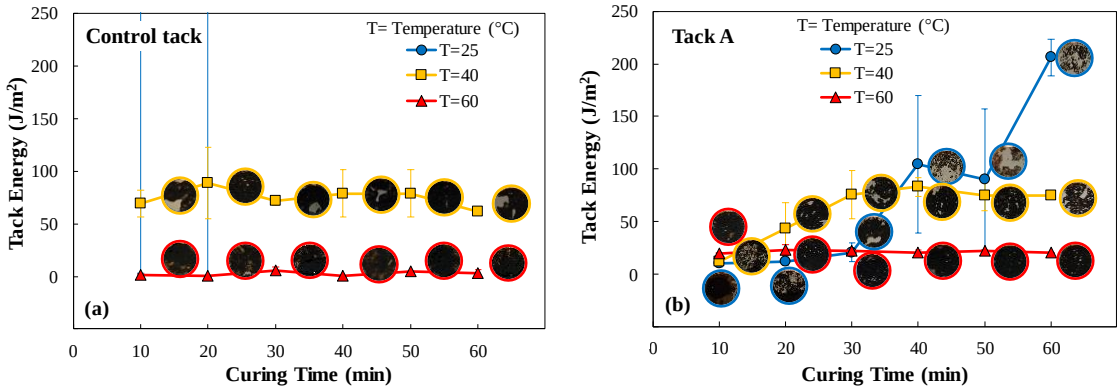

Figure 20 Tack energy at different curing time for emulsions: (a) control tack, (b) Tack A, (c) Tack B, (d) Tack C, (e) Tack D, (f) Tack E, and (g) Tack F.

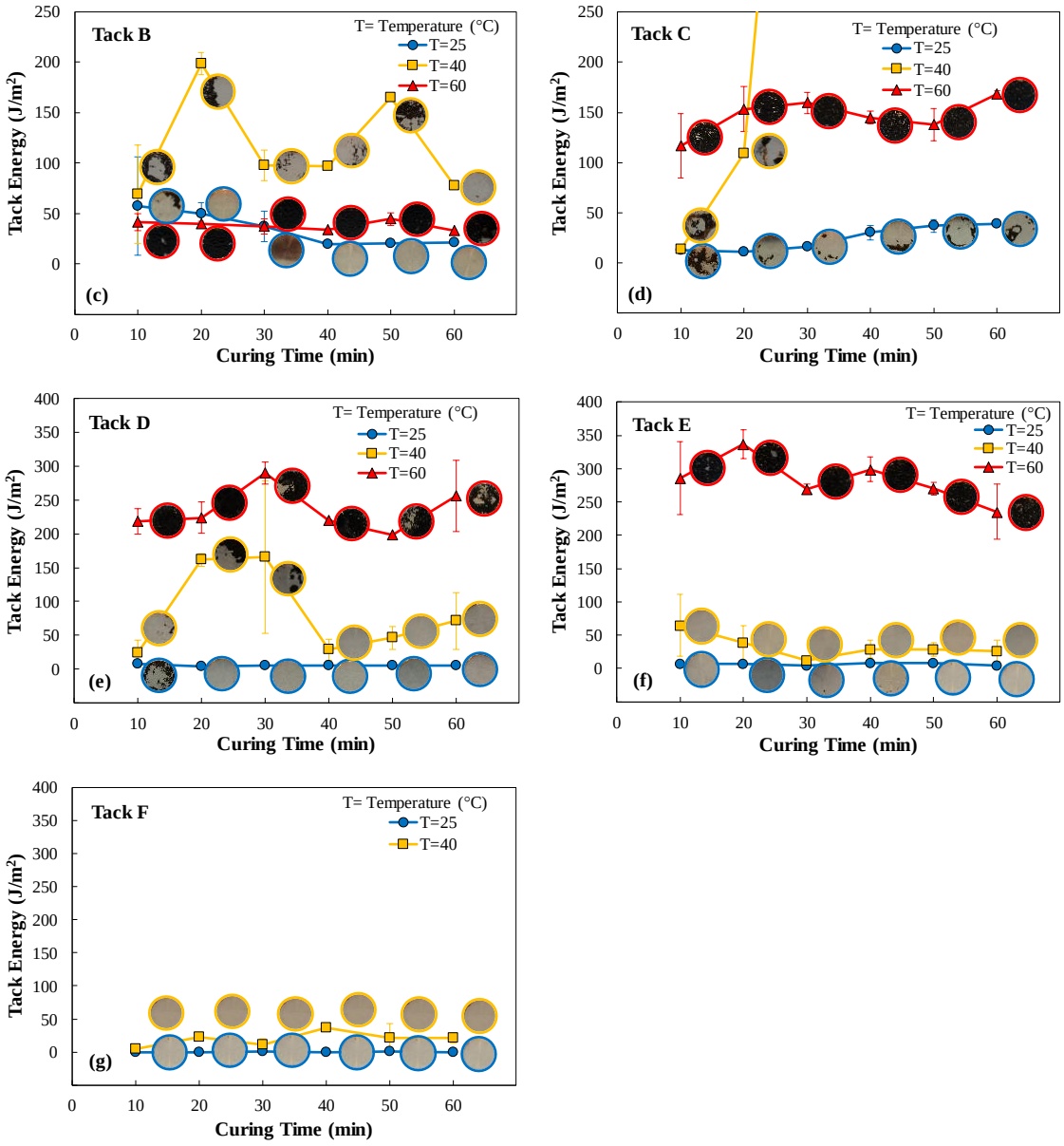

Figure 20 Continued.

Tackiness of Tack Residue

Effect of Temperature on Tackiness

The effect of temperature on tackiness is presented in Figure 21. Figure 21(a) describes the change in tack energy and failure mode of Tack B over different temperatures at constant bonding and debonding rates of 1 mm/sec. At lower temperatures, the tack was solid-like so adhesive failure was governed without a tracking issue. The temperature below 20°C belongs to the zone where tracking and change in thickness do not happen. When the temperature was raised up to about 28°C, the tack became sticky like a gum with an increase in tack energy, but it still showed a clean DSR tip surface indicating satisfactory tracking resistance of the tack material. After the magnitude of tack energy approached a maximum value, the partially cohesive failure was observed. Around the region where alteration of a failure mode occurred, a considerable change of tackiness was observed. As the temperature increased, it was observed that the tip squeezed out the asphalt sample, and consequently the thickness of the sample decreased under loading. The tack energy sharply decreased, and the dirty region of tip became larger. At temperatures higher than 40°C, the tack became liquid-like and the tip was fully covered with the tack, which was an undesired result. In addition, the tack energy did not change significantly. Since the temperature influences the rheology, viscosity, and film thickness of the asphalt sample, the temperature has a significant impact on tackiness and tracking resistance.

Figure 21(b) shows the comparison of trackless tacks and a control tack in terms of tack energy and tracking resistance. It should be noted that unfilled and filled markers

indicate a clean tip and a contaminated tip shown after testing, respectively. It was observed that all tack samples adhesively failed at lower temperatures (zone I). At temperatures between 20 and 28°C (zone II), the control tack became sticky, but the others did not track. Tack B started tracking in zone III while Tack C adhered to the probe at the temperature range in zone IV. In zone V where the temperature is over 40°C, all tacks including Tack E showed tracking, and the control tack became a viscous liquid with little cohesion. As a consequence, Tack E exhibited the highest tracking resistance, followed by Tack C and control tack.

The change in tackiness over temperatures in this study is somewhat different from the work done by Gorsuch et al. (2013). The result of the previous study that the tackiness continuously increases with temperature was valid only for adhesive failure. It was seen in this study that the tackiness decreases with temperature for the samples showing cohesive failure. Therefore, it could be concluded that the effect of temperature on the change in stickiness is different depending on the failure mode. Also, the sample with adhesive failure could be sticky while the sample with cohesive failure could exhibit low stickiness or tack energy.

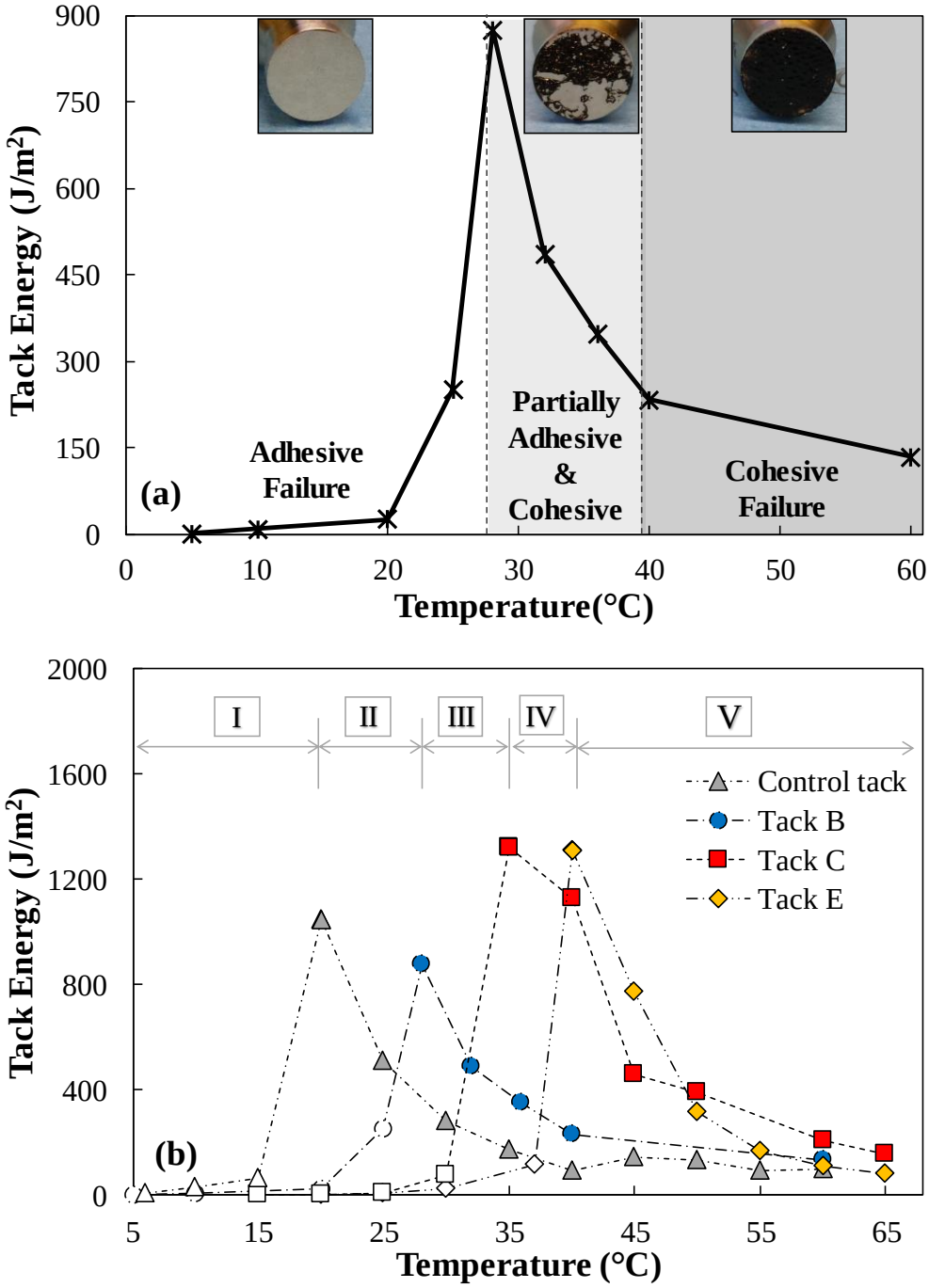

Figure 21 Effect of temperature on tack energy: (a) Tack B with observed failure modes and (b) all tacks.

Figure 22 presents the tack energy of all residue samples tested at three different temperatures. There were clear distinctions between the soft group (Control tack and Tack A, B, and C) and the stiff binder group (Tack D, E, and F) with respect to the changes in their tack energy and failure modes over different testing conditions. At 25ºC [Figure 22 (a)], the residue of trackless tack materials rarely adhered to a tip indicating adhesive failure. However, the soft group had a higher tack energy than the stiff group. The result of Tack C was closer to the stiff binder group.

As the temperature increased to 40ºC [Figure 22(b)], the soft binder group exhibited cohesive failure. In this group, higher stiffness resulted in increase in tack energy. Tack C was in this condition where the cohesive and adhesive failures were combined, thereby showing a much higher tack energy than other tacks. On the contrary, the stiff group still had adhesive failure with a slight increase in tack energy. It was observed that the control tack with different failure mode from the stiff group also had low stickiness, which emphasizes that using only the tack energy is not suitable to determine tracking resistance.

All tacks including both soft and stiff groups became soft and fluid like at 60ºC [Figure 22(c)], showing a cohesive failure. Although the soft group was less sticky than the stiff group with respect to tack energy, high tack energy in cohesive failure is more acceptable for trackless tack than low energy in such condition. In the lab, the tack sample is tested with a stainless steel probe tip while the tack interacts with a rubber tire during construction. The lab condition represents more harsh condition compared to the field since the tack-steel adhesive bond is likely higher than the tack-rubber adhesive

bond, as described in Table 8. Therefore, tacks that have a high energy with cohesive failure in the lab could have adhesive failure (trackless properties) in the field. The rank of tack energy at 60ºC was matched with the rheological properties for all tacks except for Tack E. Furthermore, it was observed that significant changes in tracking of the soft group occurred between 25 and 40ºC, and for the stiff group between 40 and 60ºC. In other words, the soft group exhibited the transition from solid-like to liquid-like behavior at a lower temperature than the stiff group.

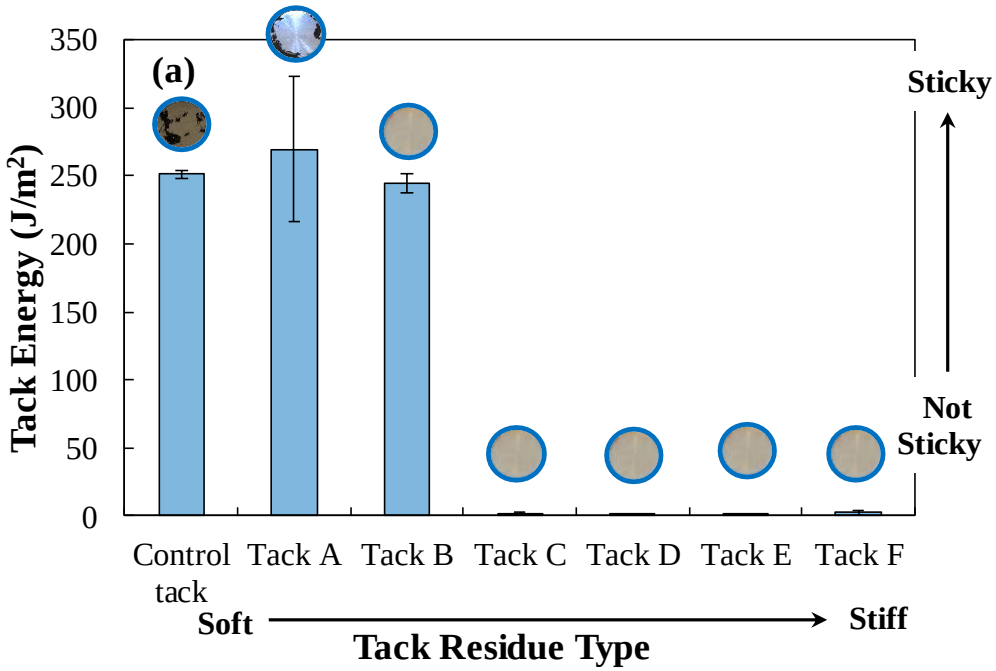

Figure 22 Tack energy of tack residues at different temperatures: (a) 25ºC, (b) 40ºC, and (c) 60ºC.

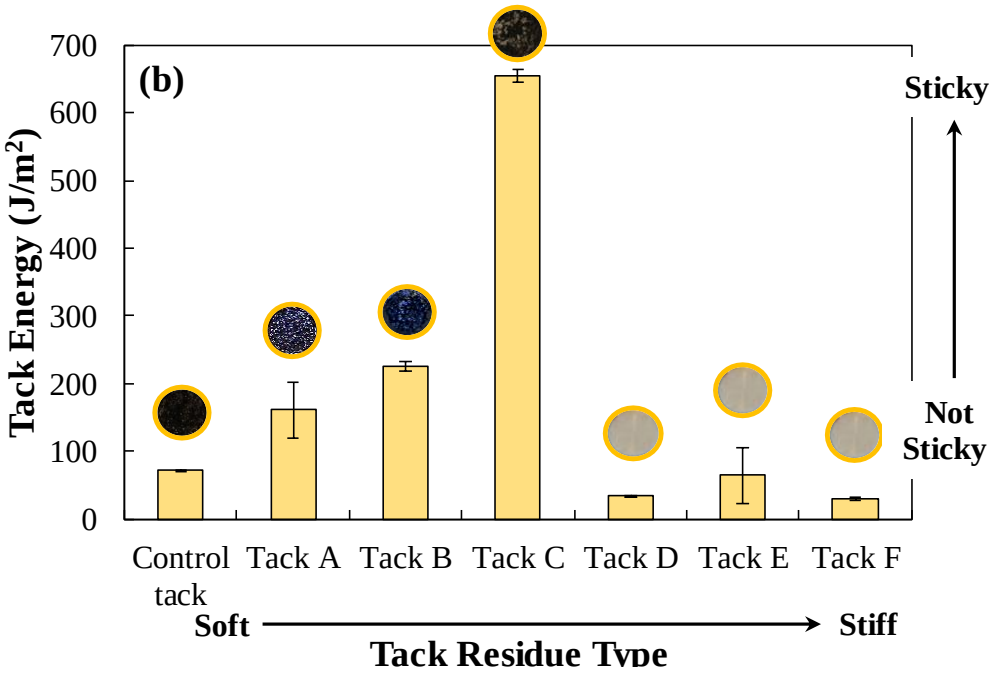

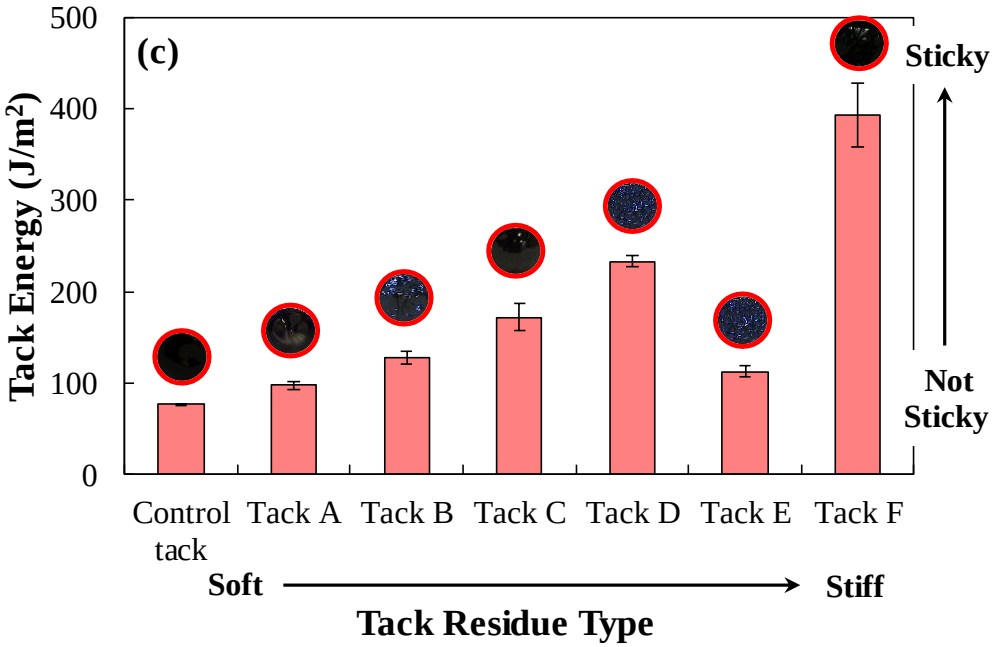

Figure 22 Continued.

Effect of Bonding/Debonding Rate on Tackiness

This study used the same speed rate of bonding and debonding in the tackiness test to follow the traffic loading. As the bonding and debonding rates are lower, the duration when a sample is in contact with a probe tip increases. In other words, lower rates allow more time for relaxation process of the sample and provide better wetting on the tip.

Figure 23 presents the effect of the bonding and debonding rates on tackiness of tack materials. The reduced speed rates were used to shift the data obtained at different temperatures using the shift factor determined through the DSR frequency sweep test. The results show that the tack energy decreased at lower speed rates when the tacks failed cohesively. At the condition where the failure mode was changed from cohesive or adhesive failure, all tacks showed the highest tack energy. At higher reduced speed rates above the region, the tacks were not prone to adhere to the tip. This trend is the same line with the result of Ondarçuhu (1997) although the previous study considered only the debonding rate.

As a consequence, each tack exhibited the change of failure mode at a different level of speed rate, and the relationship between the speed rate and tack energy could be predicted by a power law. This result would be helpful in determining the tracking resistance at a given condition.

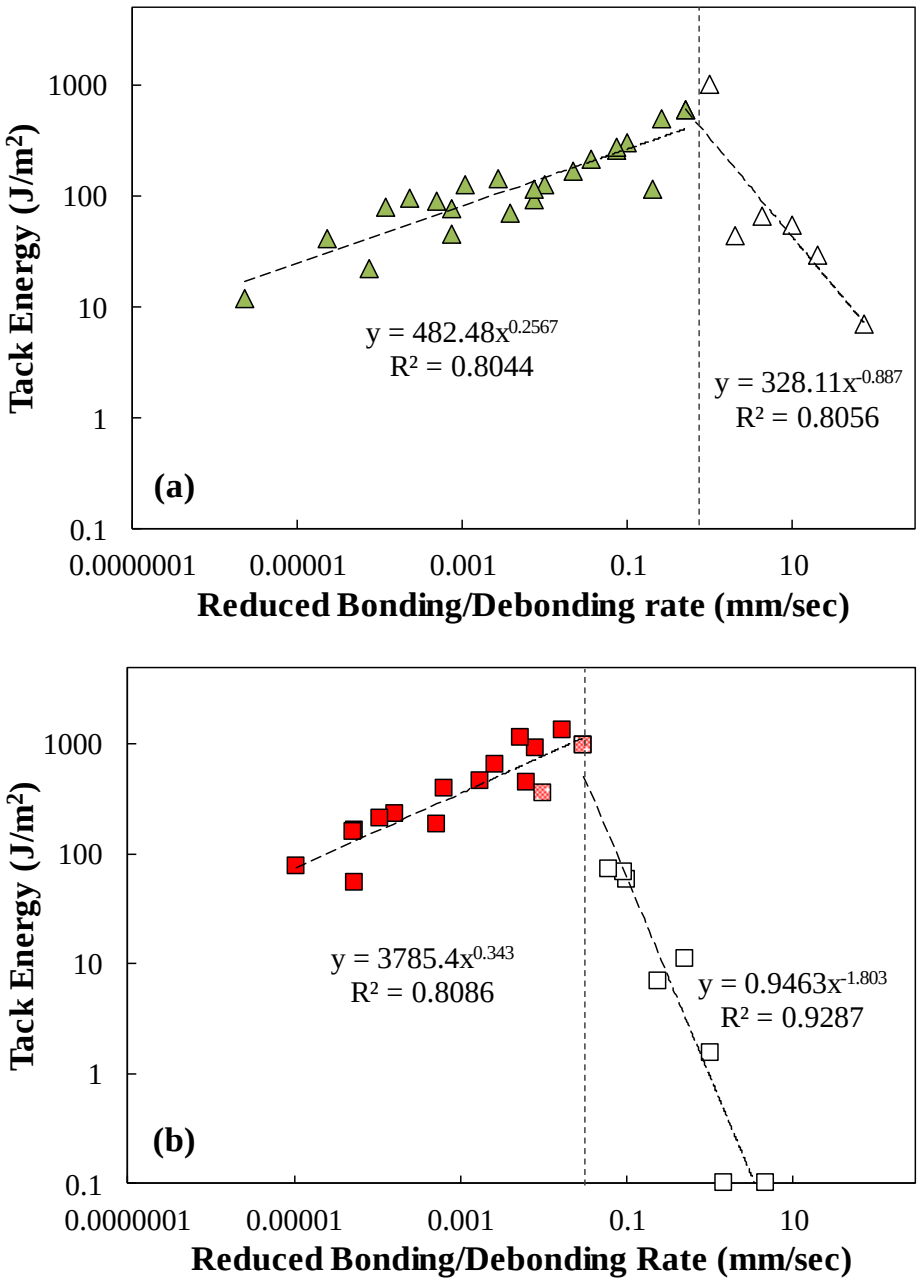

Figure 23 Tack energy of tack coats at different bonding/debonding rates: (a) Control tack, (b) Tack C, and (c) Tack E.

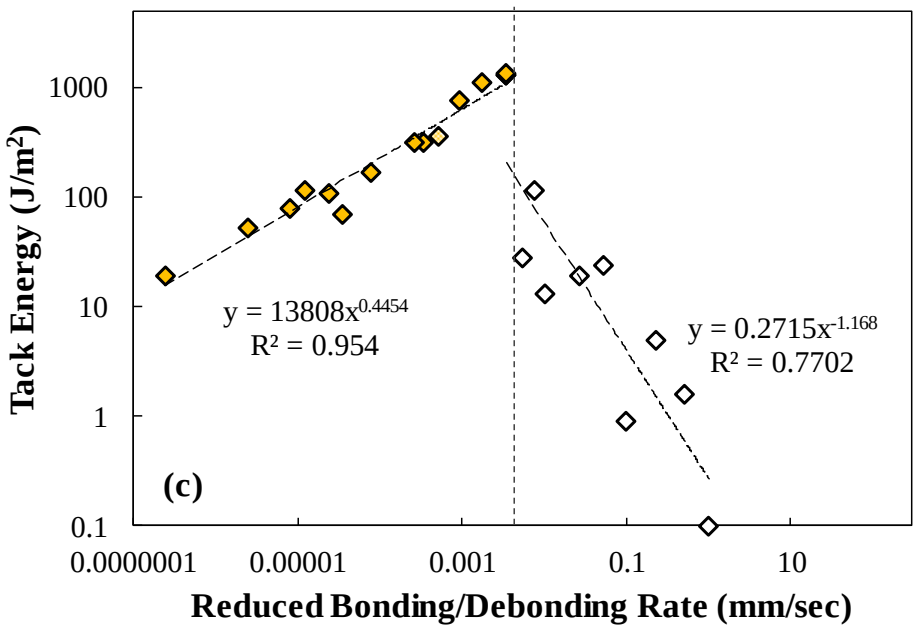

Figure 23 Continued.

Direct Shear Test Results

Tack Type of Laboratory Compacted Specimens

Different factors affecting shear bonds are evaluated and illustrated in this section. Figure 24 and Figure 25 display the results of the direct shear test on laboratory compacted samples to reflect the effect of tack type on shear bonds. As given in Figure 24(a), there was no significant difference in shear bond strength of tack samples. The shear bond strength of No Tack sample was slightly lower than that of other samples. However, all samples including No Tack sample had excellent bonds over 1,000 kPa. This level is about 45 percent higher than the minimum strength of 689 kPa suggested by West et al. (2005). In Figure 24(b), No Tack sample exhibited lower shear bond energy than the other tack samples. Among the samples applied with tacks, Tack A sample had

the lowest shear bond energy, followed by tack samples in the soft-residue group, and Tack E sample achieved the highest shear bond energy.

The difference in energy between samples having similar bond strength is associated with a crack growth path. It was noted that the red marked areas indicate the failure through the overlay mixture. As seen in Figure 25(a), No Tack sample and tack samples in the soft-residue group were prone to fail at the interface, showing few fragments of the overlay mix at the edge of substrates. It implies that tacks in the soft-residue group had a weak bond between the overlay and substrate layers. In contrast, Tack D and E samples in the stiff-residue group mostly failed within the overlay, as highlighted with a red marker in Figure 25(b). Therefore, the shear bond energy was considered as a useful measure to evaluate the interlayer shear resistance of tacks. This could be useful especially for asphalt mixtures having similar bond strength and different failure locations (i.e. along interface or through mix).

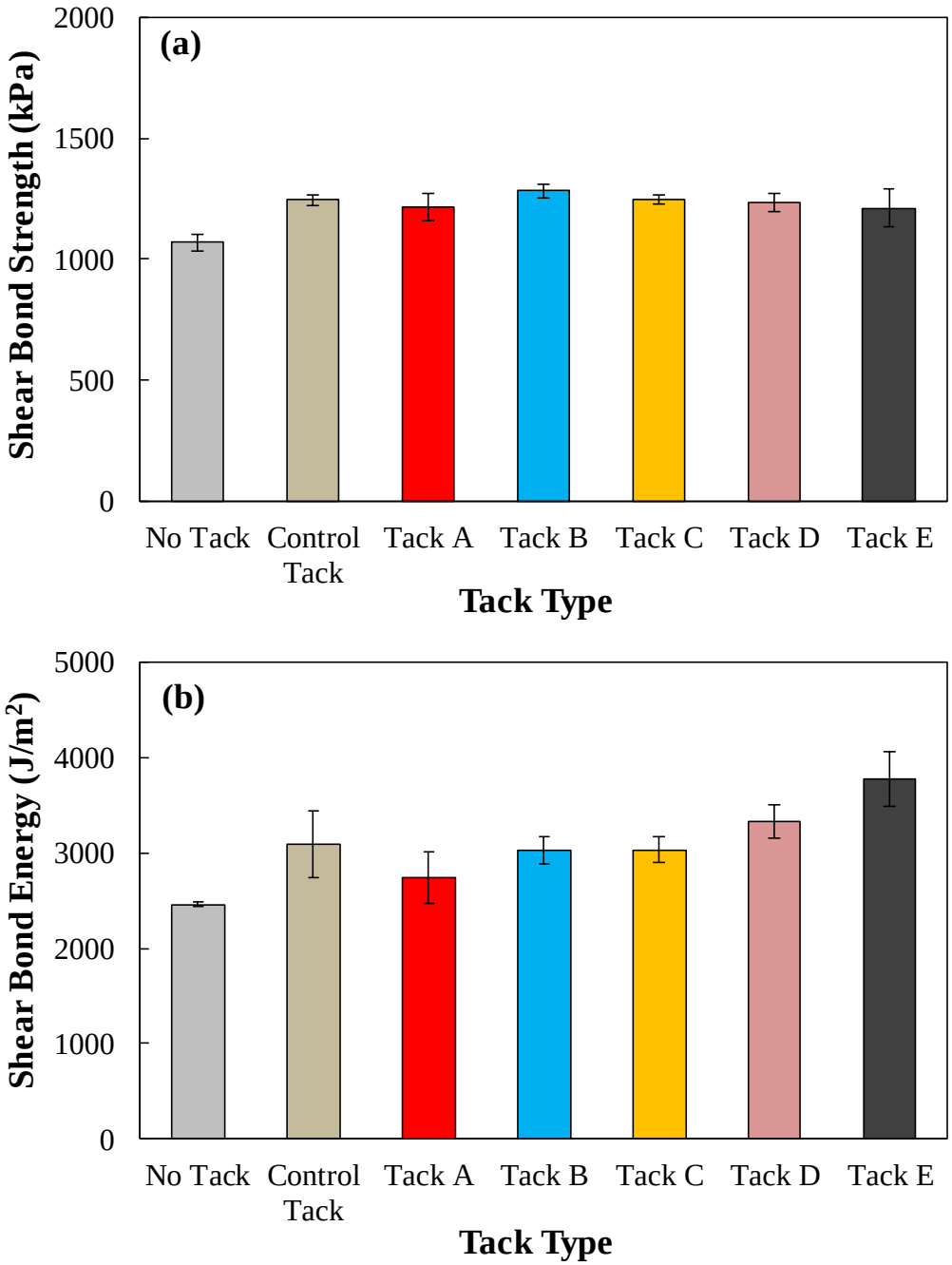

Figure 24 Effect of tack type on (a) shear strength and (b) shear bond energy for laboratory compacted samples.

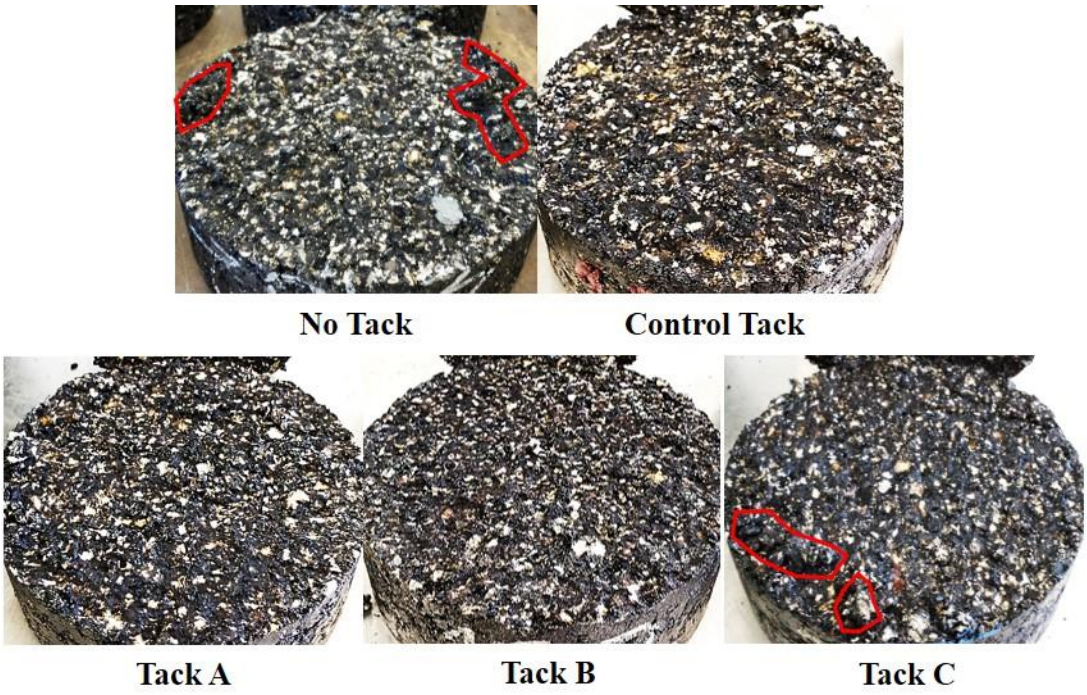

(a) Soft binder group

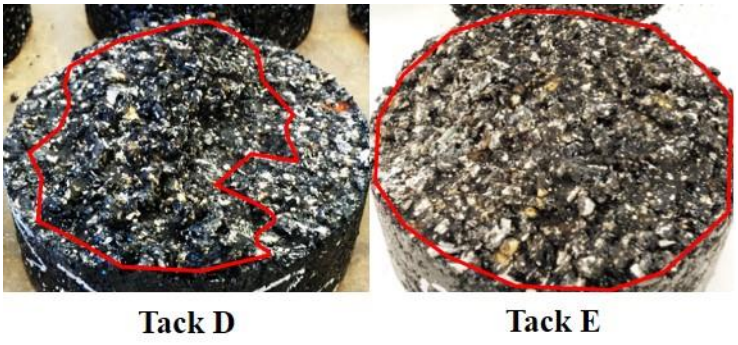

(b) Stiff binder group

Note: Red marked areas indicate the failure through the overlay mixture

Figure 25 Failure location for laboratory compacted samples applied with different tacks: (a) soft binder and (b) stiff binder groups.

Substrate Type of Laboratory Compacted Specimens

Figure 26 and Figure 27 show the results of the laboratory compacted samples with No tack and Tack D, indicating the influence of substrate type on interlayer shear resistance. For samples without tack, the concrete substrate showed extremely low shear bond strength and energy than the HMA substrates, as shown in Figure 26(a) and (b). In a comparison between two HMA substrates, polishing the laboratory prepared HMA surfaces did not affect the shear bond strength and energy. The application of Tack D on the HMA and concrete substrates provided higher shear resistance in terms of strength and energy, and the improvement of bonding on the concrete substrate was remarkable.

For two HMA substrates presented in Figure 27(a) and (b), an interface failure was dominant for No Tack samples, while major cracks propagated through the overlay in Tack D samples. On the contrary, interface debonding occurred on the concrete substrate regardless of tack application, as shown in Figure 27(c).

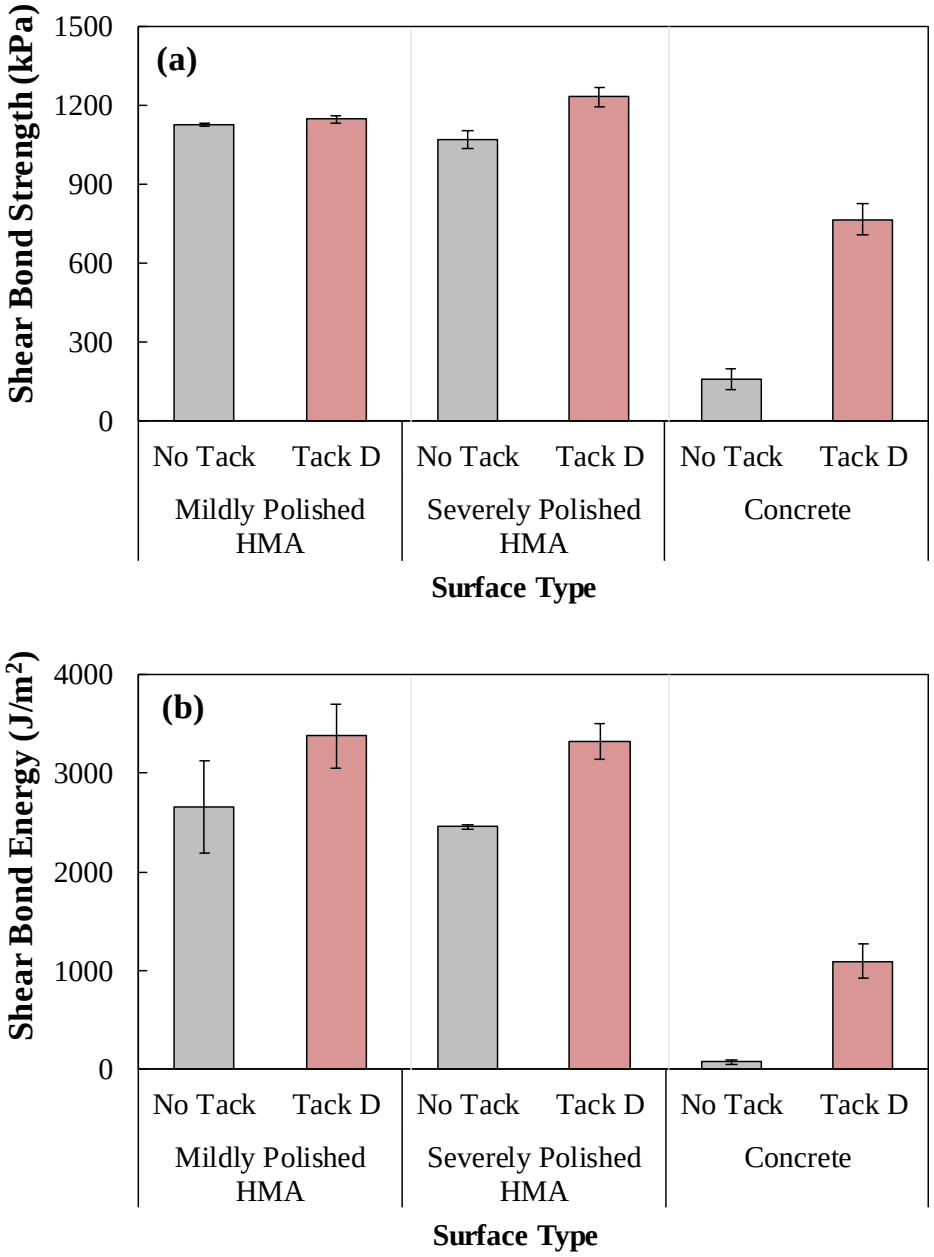

Figure 26 Effect of substrate type on (a) shear strength and (b) shear bond energy.

No Tack Tack D

(a) Mildly Polished HMA

No Tack Tack D

(b) Severely Polished HMA

No Tack Tack D

(c) Portland Cement Concrete

Note: Red marked areas indicate the failure through the overlay mixture

Figure 27 Shear failure of laboratory compacted samples without tack and with Tack D on different surfaces: (a) mildly polished HMA, (b) severely polished HMA, and (c) Portland cement concrete.

Tack Reactivation Temperature of Laboratory Compacted Specimens

The effect of tack reactivation temperature on interlayer shear resistance of laboratory samples with different tacks is described in Figure 28. The tack reactivation temperature used in this study is defined as the average of the substrate temperature and the compaction temperature of the overlay mixture. At lower temperatures, all samples were broken at the interface. With the increase in temperature, a partial or complete failure in the mix was observed for four specimens (i.e. Tack D and E samples at 87°C, and Tack C and D samples at 95°C). Obviously, higher tack reactivation temperature increased the adhesion of tacks to adjacent layers, which results in higher shear bond strength and energy for all samples including No Tack sample. At the tested temperature range, Tack E and No Tack samples exhibited the highest and lowest shear bond strength and energy, respectively. Tack C had higher shear bond strength but may exhibit inferior fatigue performance in traffic loading than Tack D.

The last variable to consider for evaluating the interlayer shear resistance for laboratory compacted samples is the compaction angle. The result shows that the shear bond strength at the compaction angle of 1 and 1.25° was 964 and 1,040 kPa, and the shear bond energy was 2,252 and 2,550 J/m^2, respectively. Lower compaction angle provided a 7 percent reduction in strength and 11 percent reduction in energy. Also, the change in compaction angle within the tested range did not affect the failure location.

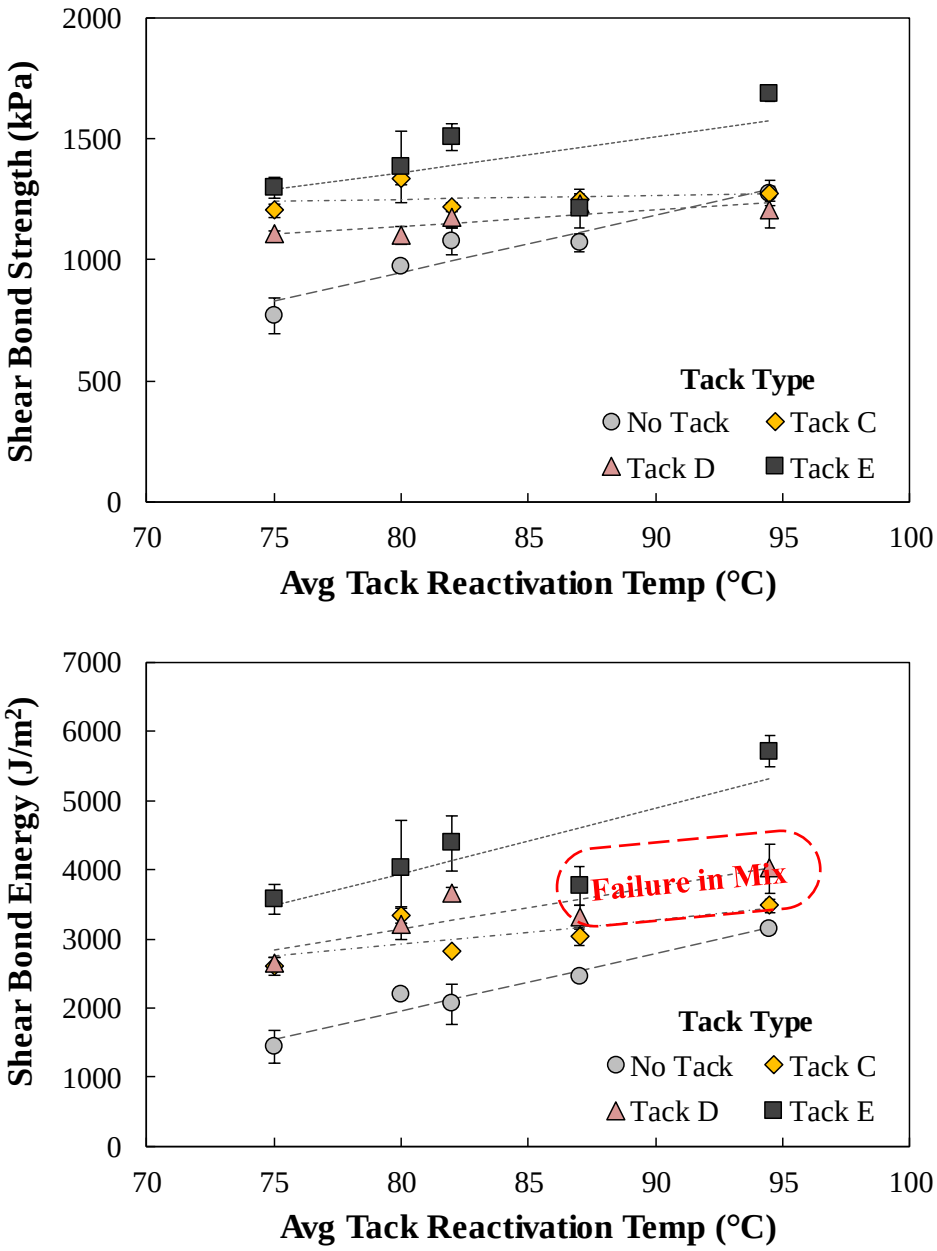

Figure 28 Effect of tack reactivation temperature on shear bond strength for laboratory samples with different tacks.

Surface and Tack Type, and Residual Tack Rate of Field Cores

The results of the direct shear test for field cores are described in Figure 29 and Figure 30. Figure 29 displays the fractured surface of field cores having different substrates. Unlike laboratory prepared specimens, all the field cores failed at the interface. It was challenging, if not impossible, to distinguish the failure mode like cohesive and adhesive failures during the test. As marked with a red marker in Figure 29(a), the brighter surface area of the existing layer was uncovered by a tack material and spotted unevenly. Figure 29(b) shows the new layer broken smoothly at the interface, and the failure mode of the new layer was not definite. Figure 29(c) shows the interface failure of the milled layer having a wavy pattern. Several bright lines on the ridge of the upper layer and the groove on the bottom layer were observed. During the milling process, fine particles were accumulated on the groove of the bottom layer, and some of the particles were picked up to the ridge of the upper layer. The loss of adhesion along the bright lines lowered the interface shear resistance of the milled layer.

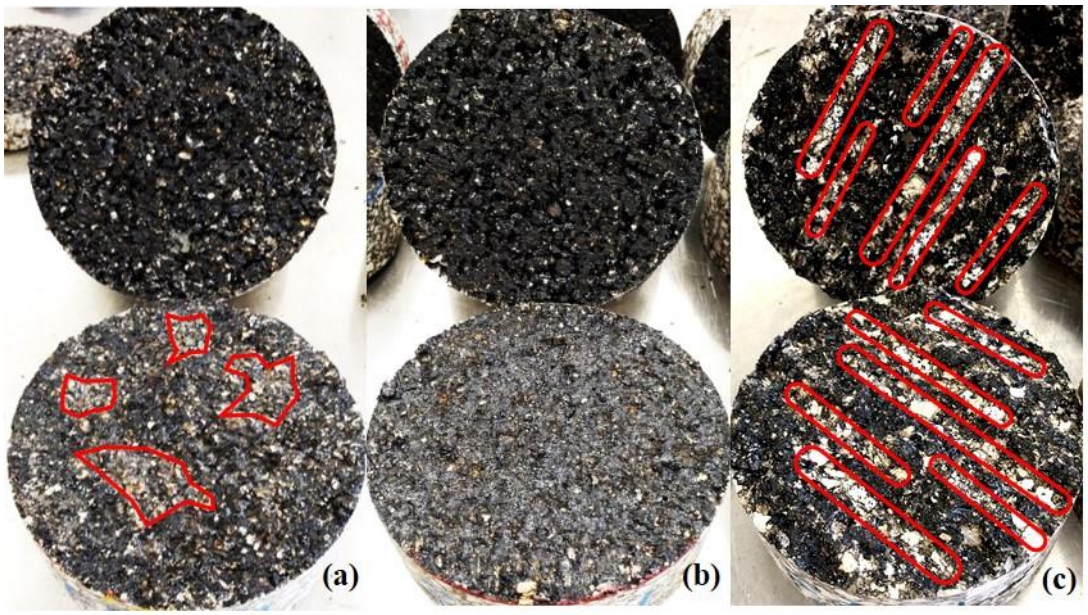

Note: Red marked areas indicate adhesive failure between tack coat and the substrate surface

Figure 29 Interface shear failure of field cores having different underlying layers in: (a) existing, (b) new, and (c) milled sections.

Figure 30 illustrates the shear bond strength of field cores to evaluate three factors (i.e., surface type, tack type, and residual tack rate) related to interface bonding. Here, the energy term was not considered in evaluating the interlayer shear resistance since the field samples failed at the interface. The field cores had considerably lower shear bond strength, of which the level is approximately 30 percent of the average strength of the laboratory compacted samples without tack treatment.

On the existing surface, as presented in Figure 30(a), Tack B treatment did not produce a substantial increase in shear bond strength, whereas Tack D dramatically improved the interface bond. Also, a moderate tack rate showed the highest bond strength, while a high rate had an adverse impact on the shear resistance. However, the

interlayer shear resistance seemed to be less sensitive to different levels of the residual tack rate than tack type.

On the new layer, as shown in Figure 30(b), the application with either Tack B or D did not significantly improve the shear bond strength. Furthermore, No Tack sample with new substrate had higher bond strength than one with existing substrate. Because an asphalt binder of the bottom layer was not severely aged, it is possible that the binders of the top and bottom layers at interface adhered to each other without tack. For the tack samples having the new surface, the shear resistance was independent of tack quantity. It was noted that the new layer had a higher sample-to-sample variance than other layers.

It is shown in Figure 30(c) that the tack application on the milled layer slightly increases the shear strength. As explained previously in Figure 10(c), some particles deposit on the groove of the bottom layer may inhibit the tacks from bonding at the interface. Thus, higher shear resistance can be achieved by eliminating dirt on the groove before tack treatment. In a comparison of No Tack samples with milled and existing substrates, the roughness of surface texture contributed to higher shear resistance by aggregate interlocking. The milled layer showed the highest shear resistance at the moderate level of residual tack rate like the existing layer.

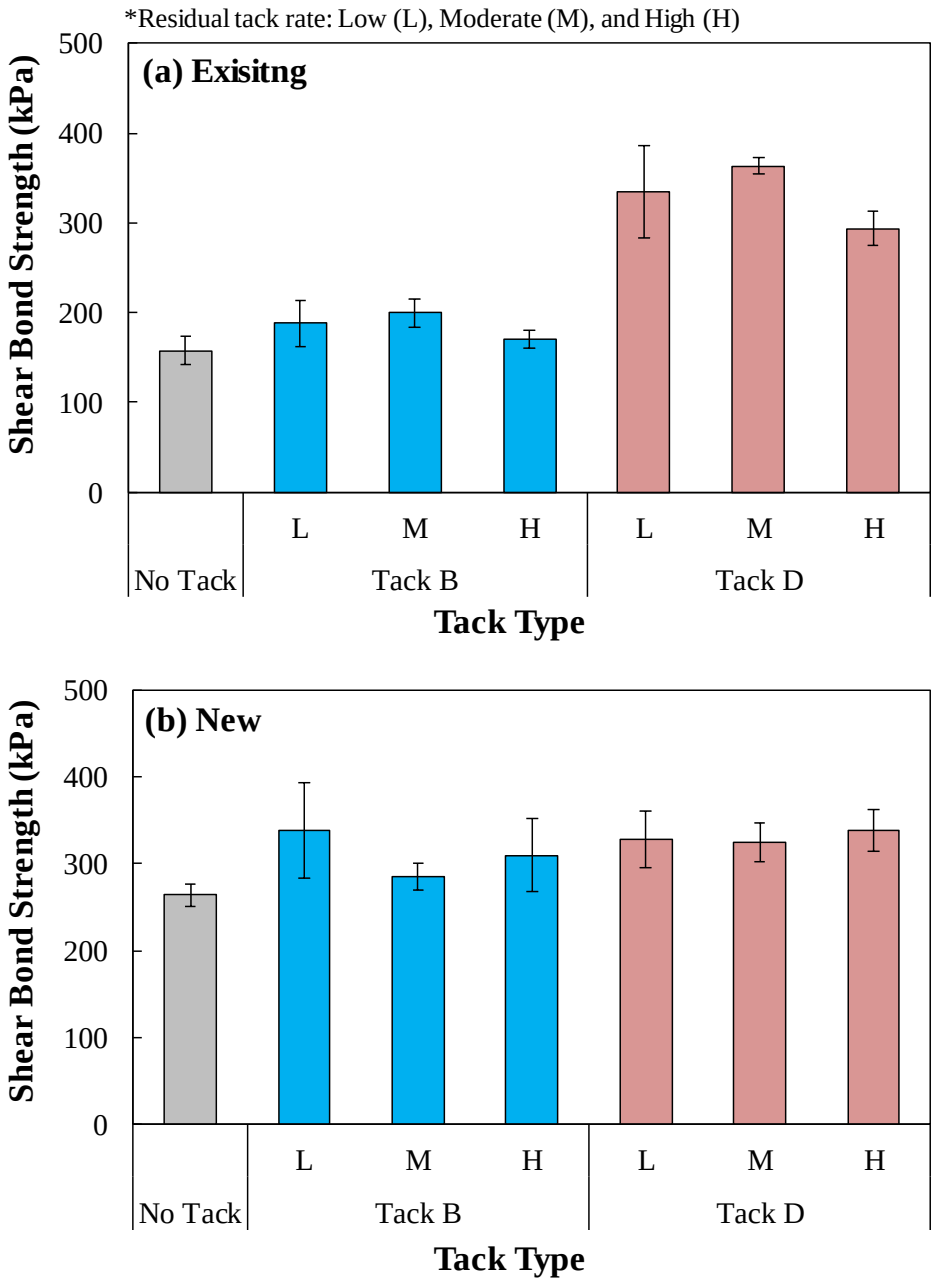

Figure 30 Effect of surface type, tack type and residual tack rate on shear bond strength for field cores with different underlying layers in: (a) existing, (b) new, and (c) milled sections.

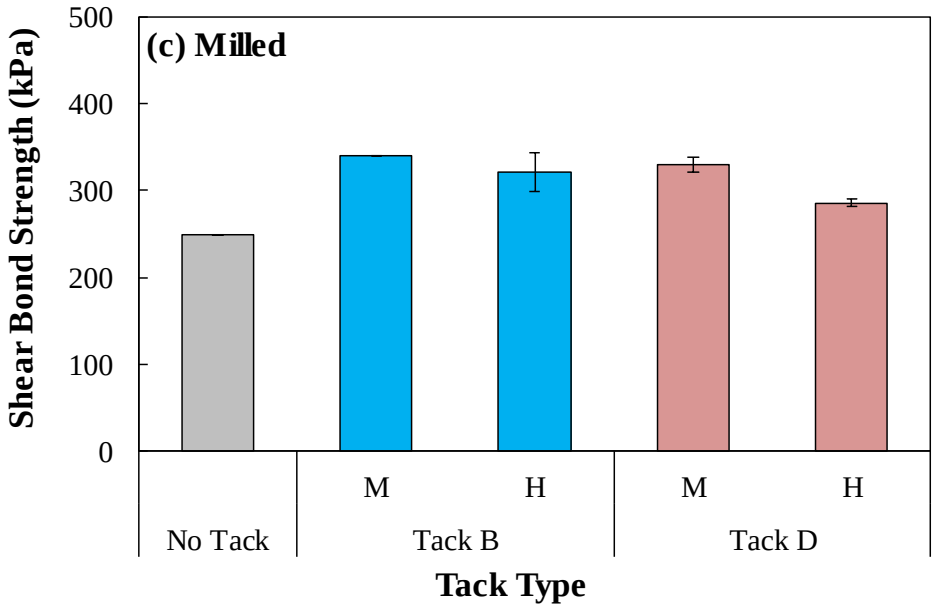

Figure 30 Continued.

The results of statistical analysis on interlayer shear resistance for each experiment are shown in Table 10. It is indicated that variables with "*" symbol have a significant effect on either shear strength or energy, and variables with "**" symbol largely influence both shear bond strength and energy. If a significance level (*p*-value) of variables is greater than 0.05, the variables can be considered unimportant and removed from the statistical models. The model with "–" symbol is void because no significant variables are present in the model. Also, two variables denoted with "×" symbol were used to examine if there is significant interaction between the variables. The presence of significant interaction means that one variable has a different impact on the shear bonding when considering different values of other variables.

The results show that tack type did not significantly affect shear resistance for samples using severely polished HMA substrate, compaction angle of 1.25°, overlay

compacting temperature of 149°C and substrate temperature of 25°C. However, tack type was a significant variable affecting both shear bond strength and energy in other experiments. Also, the surface type and tack reactivation temperature made an important contribution to both shear bond strength and bond energy. The sensitivity of shear bond strength to tack type was different depending on tack reactivation temperature and surface condition. The effect of compaction angle on shear bond energy, while statistically significant, was not as critical as that of tack type and temperature. Therefore, this variable was considered to have only a marginal effect on bond performance.

In the field experiments, the effect of residual tack rate on shear bond strength was not statistically significant. This consequence may be due to other surface conditions like dirt and moisture, which were not considered in this study. Also, the low number of replicates for tack rate may be another reason for the low significance level of tack rate on bonding. Based on the limited test results, it could be concluded that tack and surface types are more influential variables than tack rate for interlayer shear resistance.

Table 10 Results of statistical analysis of shear bond strength and energy.

Experiment	Explanatory Variable	Shear Bond Strength			Shear Bond Energy		
		Variable *p*-value	Model *p*-value	Model R^2	Variable *p*-value	Model *p*-value	Model R^2
Laboratory Compacted Samples							
Tack Type	Tack	>0.05	–	–	0.05	0.05	0.57
Substrate Type	Tack**	<0.001	<0.001	0.98	0.001	<0.001	0.95
	Substrate**	<0.001			<0.001		
	Tack×Substrate*	<0.001			>0.05		
Tack Reactivation Temperature	Tack**	<0.001	<0.001	0.85	<0.001	<0.001	0.87
	Temp**	<0.001			<0.001		
	Tack×Temp*	<0.001			>0.05		
Compaction Effort	Comp. Angle*	0.05	<0.001	0.74	0.02	<0.001	0.86
	Tack**	<0.001			<0.001		
	Temp**	<0.001			<0.001		
	Comp.angle×Temp	>0.05			>0.05		
	Comp. angle×Tack	>0.05			>0.05		
Field Cores							
Residual Tack Rate	Rate	>0.05	<0.001	0.68	>0.05	<0.001	0.79
	Tack**	<0.001			<0.001		
	Surface**	0.001			<0.001		
	Rate×Tack	>0.05			>0.05		
	Rate×Surface	>0.05			>0.05		
	Tack×Surface*	0.001			>0.05		

Note: * Variables that have significant effect on either shear bond strength or energy.

** Variables that have significant effect on both shear bond strength and energy.

>0.05 Variable not significant and removed from the model.

– Value not calculated.

× Two variables considered to examine their interaction effect.

CHAPTER V

NUMERICAL DAMAGE MODEL FOR TRACKING

Tracking of tacks to vehicle tires shall be prevented to minimize the loss of tacks and provide the required bonding between overlay and underlying layers. Currently, various test methods for assessing the tracking resistance of trackless tacks have been established, and new trackless tacks have been introduced in an effort to reduce the tracking issue. However, the mechanisms leading to tracking of tacks have not been well understood. Thus, the focus of this chapter is to discuss the mechanisms responsible for tracking and develop a damage model to characterize the material properties related to microcracking.

Associated Mechanisms in Contact and Fracture Processes

Tracking of tacks is strongly related to mechanisms that occur in asphalt mixtures subjected to fatigue loading. Little et al. (2001) addressed three mechanisms (i.e., relaxation, fracture, and healing): relaxation mechanism determines the stress response of an asphalt structure, and the damage of asphalt mixture is induced by the growth of microcracks or macrocracks. During rest periods, the asphalt molecular structure at crack closure is recovered by the healing mechanism.

Figure 31 depicts the main processes that occur while a vehicle tire rolls over a tack layer in the field (top) or the DSR tackiness test is conducted in laboratory (bottom). The first step that the tacks undergo is the contact process. In this process, the pressure is

distributed at the interface between the tack and adherends (i.e., rubber tire or stainless steel tip). The tack is relaxed and keep wetting on the surface of the adherends. Lytton (2000) demonstrated that the rate of healing is in good relations with the surface energy component of asphalts. An initial healing rate is inversely related to the dispersive surface energy component, and an ultimate healing is directly related to the polar surface energy component. It was also found that healing is dependent on the length of the rest period, the temperature during the rest period, and the type of asphalt mixture. Since the contact process is associated with the relaxation and healing mechanisms, various factors (i.e., loading rate, compressive force, resting time, and the type of adherends) may be dependent on the contact quality of the tacks with the adherends.

Another step is the fracture process while the tack is debonded from the adherends. During the debonding process, the initiated cracks propagate or the fibrillar structures will be formed (Zosel 1989, Zosel 1998). The deformation and crack propagation rates are controlled by the vehicle speed. Like the tire movement, the tip was pulled off from the tack sample at the same rate of loading. From the tackiness test results conducted at various loading rates and temperatures, the fracture properties of the tack materials can be determined on the basis of the fracture mechanics methodology.

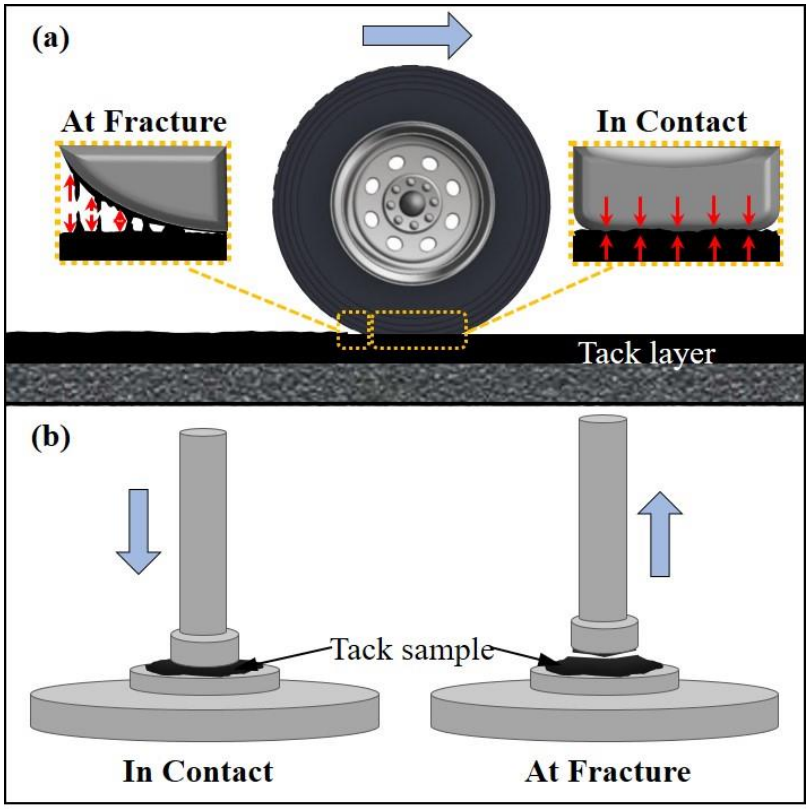

Figure 31 Schematic picture of tracking process in: (a) field and (b) laboratory test.

A well-known damage model is the Paris's law established by Paris and Erdogan (1963). For a linear elastic material, the relationship between the crack growth rate and the stress intensity during crack propagation is defined as:

$$\frac{dc}{dN} = AK^n \tag{16}$$

where, c is crack length, N is the number of loading cycles, A and n are the Paris' law coefficient and exponent and dependent on material properties and test conditions. K is the stress intensity factor and describes the stress state near the crack tip. Later, Cherepanov (1967) and Rice (1968) introduced *J*-integral that is a path-

independent line integral around the crack front. The physical meaning of the *J*-integral represents the energy release rate per unit area of a crack. For a nonlinear elastic material that undergoes a plastic deformation, the *J*-integral can be applied to the damage model instead of the stress intensity factor (Dowling and Begley 1976).

The theory of viscoelastic fracture to predict the initiation and propagation of cracks was developed by Schapery (1975) and has been successfully used to predict the fatigue cracking of asphalt mixture (Lytton et al. 1993). Schapery (1984) also suggested the correspondence principle to reduce a viscoelastic problem into an elastic problem with the use of pseudo variables. Si et al. (2002) extended this concept to describe the nonlinear behavior of the asphalt material.

Recently, Luo et al. (2013) modified the Paris's law formulation of Equation (16) by introducing the damage density to predict numerous cracks. The damage growth rate in asphalt mixtures subjected to fatigue loading can be expressed as:

$$\frac{\partial \Phi(t)}{\partial N} = A'[J_R]^{n'} \tag{17}$$

where, Φ is the damage density and indicates the degree of a damaged area to an initial contact area, ranging from 0 to 1. A' and n' are the modified Paris' law coefficient and exponent. The pseudo *J*-integral is defined as the rate of change in dissipated pseudo-strain energy per unit area of a crack as follows:

$$J_R = \frac{\partial W_R}{\partial csa} = \frac{\partial W_R / \partial t}{\partial csa / \partial t} \tag{18}$$

in which, W_R is the dissipated pseudo-strain energy, and csa is the crack surface area. The pseudo *J*-integral is a parameter to characterize the fracture that controls the crack growth whereas the dissipated pseudo-strain energy is an important quantifier to describe the damage and characterize the fracture properties of a material. The crack surface area can be expressed in terms of damage density as follows:

$$csa(t) = 2\pi a^2 \Phi(t) \tag{19}$$

where, a is the radius of an initial contact area. For a monotonic tensile loading, the crack growth rate per load cycle in Equation (17) can be replaced with the damage density rate with time. Based on the modified Paris's law proposed by Luo et al. (2013), the damage density growth can be rewritten in the following simple form:

$$\frac{\partial \Phi(t)}{\partial t} = A'^{\frac{1}{n'+1}} \left[\frac{1}{2\pi a^2} \frac{\partial W_R}{\partial t} \right]^{\frac{n'}{n'+1}} \tag{20}$$

Using the Paris's law parameters A' and n' in Equation (20), the material properties related to the fracture resistance were obtained from the tackiness test in this study.

Stress Response in Tackiness Test

The stress response of a linear viscoelastic material to an arbitrary strain history is mathematically constructed in an accordance with Boltzmann superposition principle as follows:

$$\sigma(t) = \int_0^t E(t-\tau)\frac{\partial \varepsilon(\tau)}{\partial \tau} d\tau \tag{21}$$

where, σ is the viscoelastic stress, and ε is the input strain. t and τ are the present time and the time when strains are measured, respectively. $E(t-\tau)$ is the relaxation modulus at a desired loading time, $t-\tau$.

The relaxation modulus can be simply defined by a power law as follows:

$$E(t) = E_\infty + E_1 \cdot t^{-m} \tag{22}$$

where, E_∞ and E_1 are the relaxation modulus coefficients, and m is the slope of the log relaxation modulus versus log time graph. The relaxation modulus can be directly obtained from the results of the frequency sweep test using interconversion methods. This is valid since the mathematical function for a linear viscoelastic material shares the equivalent information on the behavior of the material between time and frequency domains (Park and Kim 1999, Schapery and Park 1999). This study selected the approximate interconversion method suggested by Schapery and Park (1999). The method can be used to convert the storage modulus in frequency domain into the relaxation modulus in time domain as follows:

$$E(t) \cong \frac{1}{\Gamma(1-n)\cos\left(\frac{n\pi}{2}\right)} E'(\omega)|_{\omega=1/t} \tag{23}$$

Where, $E(t)$ is the relaxation modulus at time t, and $E'(\omega)$ is the storage modulus at an angular frequency ω. Γ is the gamma function, and n is the local log-log slope of E' versus ω. Since the frequency sweep test conducted in this study induces a shear stress instead of a uniaxial tensile stress, the storage modulus E' is obtained from the shear storage modulus G' through the following relationship:

$$E = 2G(1+\nu) \tag{24}$$

where, ν is the Poisson's ratio and assumed to be 0.5. E is the uniaxial tensile modulus, and G is the shear modulus. The shear storage modulus G' is calculated with the complex shear modulus G^* and the phase angle δ as follows:

$$G' = \left|G^*\right| \times \cos(\delta) \tag{25}$$

Using the results of the frequency sweep test, the relaxation modulus for tacks were calculated by the interconversion, and its coefficients are given in Table 11.

Table 11 Coefficients of relaxation modulus for tacks.

Tack	E_∞	E_1	m
Control tack	0.0182	137.9	0.9883
Tack C	0.0809	2721	0.8345
Tack E	0.0066	24810	0.9472

The force history over time is recorded in the tackiness test, as displayed in Figure 32. After the sample is compressed during the holding time, a probe tip continues to pull up the sample during the time $t_b \sim t_e$. Here, t_b is the time when the equipment starts pulling up, and t_c is the time at which the samples is loaded in a tension mode and transiting from a compression mode. t_d is the time when the tensile force reaches a peak point. t_e is the time when the tensile force approaches zero. From the stress response of the sample, the damage region was divided by point d. During the time $t_c \sim t_d$, the tacks are considered in the undamaged region where the tack sample is fully contacted to the probe tip and no crack occurs. The damaged region during the time $t_d \sim t_e$ involves crack propagation, leading to the reduction in contact area. Thus, the fracture properties of tack samples are determined using the stress response in the damage region.

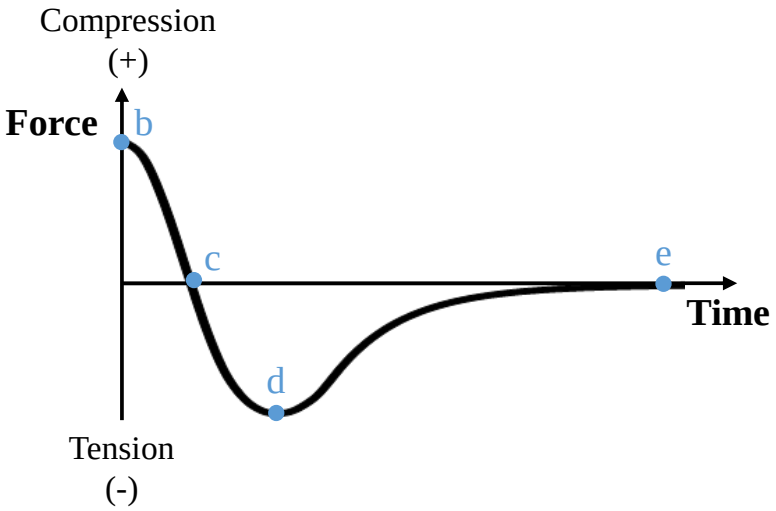

Figure 32 Force history over time in the tackiness test.

Stress Before Damage Initiation

The measured tensile stress during the time $t_c \sim t_d$, in which no damage occurs, is described as:

$$\sigma(t) = \frac{F(t)}{\pi a^2} \tag{26}$$

where, $F(t)$ is force history over time, and a is the radius of the probe tip. For the sample subjected to a displacement-controlled loading, the tensile strain is governed by the following equation:

$$\varepsilon(t) = \frac{\delta(t)}{d_t} = \frac{r \cdot t}{d_t} \tag{27}$$

where, δ is the deformation, and r is the debonding rate. d_t is the film thickness. Equations (22) and (27) are substituted in Equation (21) and the calculated tensile stress can be rewritten in another form as:

$$\begin{aligned} \sigma(t) &= \int_{\tau=t_c}^{\tau=t} \left[E_\infty + E_1 (t-\tau)^{-m} \right] \frac{r}{d_t} d\tau \\ &= \frac{r}{d_t} \left[E_\infty (t-t_c) + E_1 \frac{(t-t_c)^{1-m}}{1-m} \right] \end{aligned} \tag{28}$$

It should be noted that the debonding rate was used at the same rate of loading in the test and may involve the effect of the contact time and separation velocity simultaneously. Also, although the same initial thickness was achieved during sample preparation, the loading and temperature conditions could change the final thickness. In other words, the samples at higher temperatures may have thinner film thickness after

loading. Since the information on the change of film thickness was not provided in this study, the final thickness was approximately estimated by setting the measured stress in Equation (26) to be equal to the calculated stress in Equation (28).

Figure 33 presents the measured stress of Tack C sample tested at 40°C and 0.01 mm/sec and its calculated stresses using the initial and adjusted thicknesses. It was seen that the calculated stress using the initial thickness is much smaller as compared to the measured stress. It indicates that the adjustment of thickness is needed to follow the response obtained from the test instead of using the initial thickness.

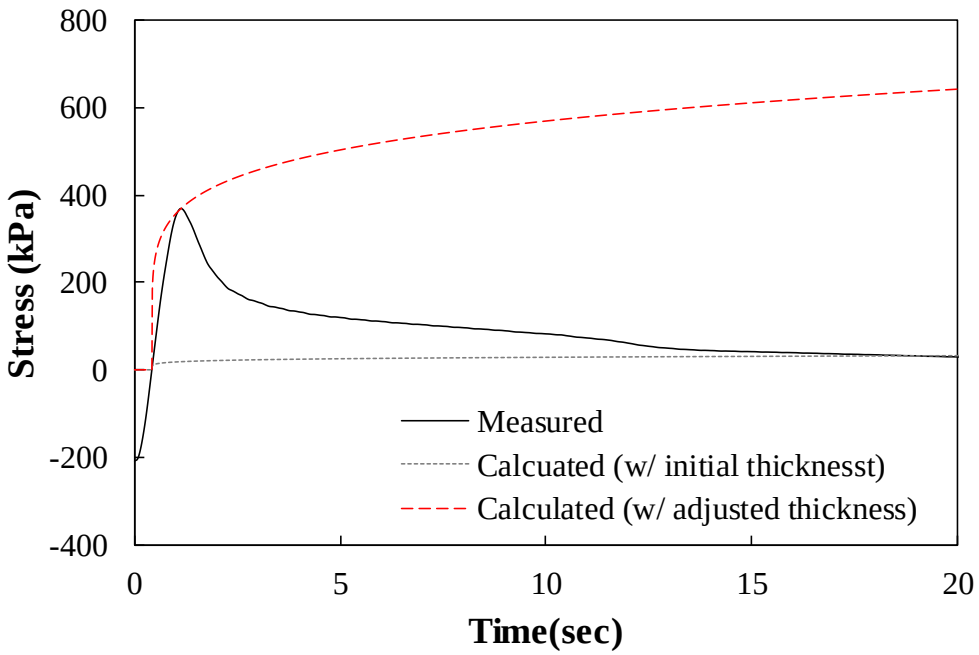

Figure 33 Comparison of the measured and calculated stresses with and without thickness adjustment.

Stress After Damage Initiation

Rate of Damage Density

In the damaged region, microcracks propagate and consequently lead to fracture. The location of crack initiation and the direction of crack propagation may affect the crack velocity. Hence, this study considers two scenarios of crack formation; (i) a crack initially occurs on the center of the sample, and then propagates outward [Figure 34(a)], and (ii) a crack starts at the edge and then grows inward [Figure 34(b)]. With the reduced contact area after damage initiation, the tensile true stress during time $t_d \sim t_e$ is expressed as:

$$\sigma(t) = \frac{F(t)}{\pi\left[a^2 - c_{in}{}^2(t)\right]} \text{ or } \frac{F(t)}{\pi\left[a - c_{out}(t)\right]^2} \tag{29}$$

where, c_{in} and c_{out} are the length of the crack that initiates at center and edge, respectively.

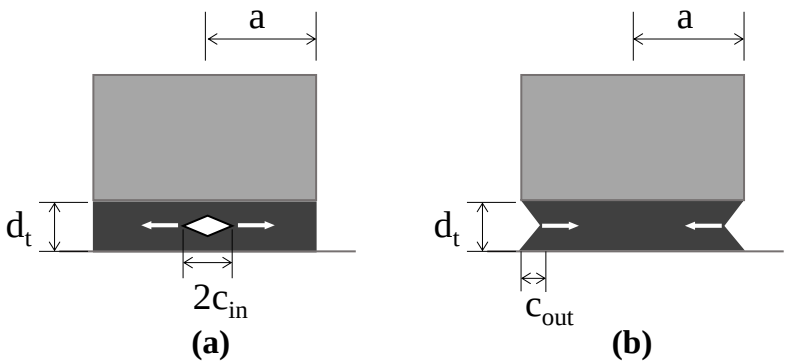

Figure 34 Location of crack initiation and propagation.

By setting the measured stress in Equation (29) equal to the calculated stress in Equation (28), the crack length can be calculated through the following equation:

$$c_{in}(t) = \left\{ a^2 - \frac{F(t)}{\frac{\pi r}{d_t}\left[E_\infty (t - t_c) + E_1 \frac{(t - t_c)^{1-m}}{1-m} \right]} \right\}^{1/2} \tag{30}$$

$$c_{out}(t) = a - \left\{ \frac{F(t)}{\frac{\pi r}{d_t}\left[E_\infty (t - t_c) + E_1 \frac{(t - t_c)^{1-m}}{1-m} \right]} \right\}^{1/2} \tag{31}$$

The damage density and its rate in the formation of microcracks are calculated through the following equations:

$$\Phi(t) = \frac{{c_{in}}^2(t)}{a^2} \text{ or } \frac{2a c_{out}(t) - {c_{out}}^2(t)}{a^2} \tag{32}$$

$$\frac{\partial \Phi(t)}{\partial t} = \frac{2c_{in}(t)}{a^2} \cdot \frac{\partial c_{in}(t)}{\partial t} \text{ or } \frac{2\left[a - c_{out}(t)\right]}{a^2} \cdot \frac{\partial c_{out}(t)}{\partial t} \tag{33}$$

If either Equation (30) or Equation (31) is substituted into Equation (33), the rate of damage density can be determined from the force history. To use the force history in the model, the raw data of force history should be smoothed to remove the noise in the data. In this study, the force curve in the damaged region is pre-smoothed using an exponential function.

Rate of Dissipated Pseudo Strain Energy

To describe a real damage and characterize the fracture properties of the tack materials, the pseudo strain is used and described as:

$$\varepsilon_R = \frac{1}{E_R}\int_{\tau=t_c}^{\tau=t}\left[E_\infty + E_1(t-\tau)^{-m}\right]\frac{r}{d_t}d\tau \tag{34}$$

where, the reference modulus E_R is introduced to eliminate the time-dependent behavior of the material. The E_R used in this study is regarded as Young's modulus measured at time t_c when the material is in linear region. The dissipated pseudo-strain energy (DPSE) represents the energy dissipated due to the fracture damage, and the rate of change in DPSE can be calculated using Equation (34)

$$\begin{aligned}\frac{\partial W_R}{\partial t} &= F(t)\frac{\partial \delta_R(t)}{\partial t} \\ &= \frac{r}{E_R}F(t)\left[E_\infty + E_1(t-\tau)^{-m}\right]\end{aligned} \tag{35}$$

where, W_R is the dissipated pseudo-strain energy and δ_R is the pseudo deformation that yields pseudo strain multiplied by the film thickness.

The rate of damage density and the rate of DPSE, which are the terms of the damage model in Equation (20), were finally calculated using Equation (33) and Equation (35). Figure 35 shows the relationship between the rates of damage density and dissipated pseudo-strain energy (DPSE) for different tacks tested at 25°C and 1mm/sec. As previously illustrated in Figure 21(b), the control tack showed high tackiness with cohesive failure while Tack C and E were non-tacky with adhesive failure. It was

indicated that the rate of DPSE increases with the damage growth rate. At the same rates of DPSE for all tacks, the control tack exhibited the lowest rate of damage growth due to its tracking behaviour. Also, Tack E had a faster damage growth rate than Tack C, which means that Tack E is more easily detached from the tip than Tack C. After the slope and *y*-intercept of the fitting curve is obtained from the relation between the rates of DPSE and damage density, the fracture parameters A' and n' of each tack can be determined by Equation (20).

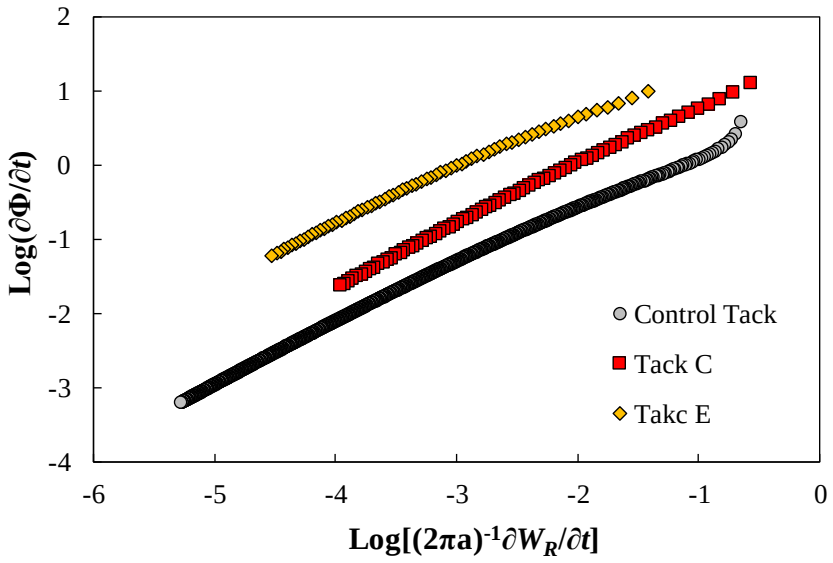

Figure 35 Relationship between the rates of damage density and dissipated pseudo-strain energy (DPSE) for different tacks.

Figure 36 presents the relationship between A' and n' obtained from the tackiness test results of all three tacks tested at various conditions. It was shown that -log A' linearly increases with n', and all tacks have a high correlation between two parameters. Also, a larger n' leads to a smaller A', which is in good agreement with

Luo et al. (2013)'s mathematical relation between -log A' and n' for different types of asphalt mixtures. However, the slope of the curves in this study was higher than the one suggested by the previous study.

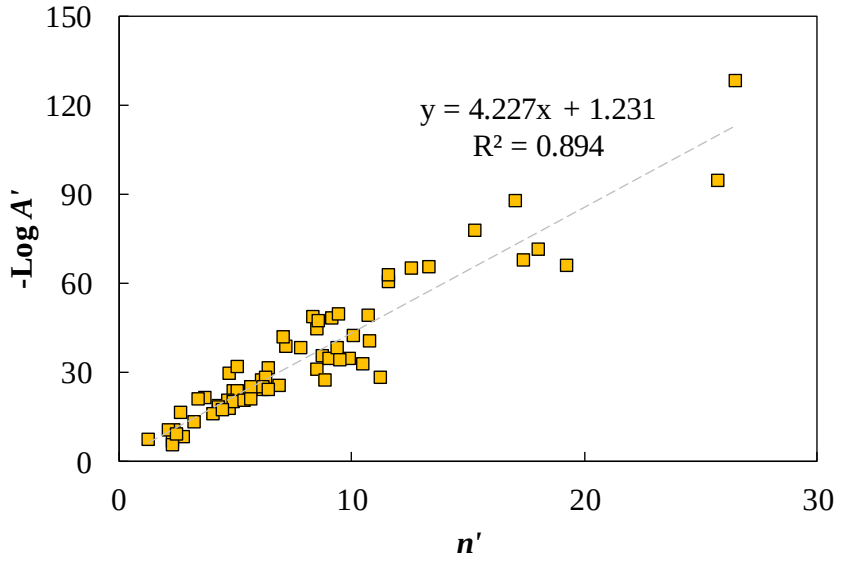

Figure 36 Relationship between fracture parameters *A'* and *n'* of all tacks.

After substituting the relationship between A' and n' into Equation (20), the damage growth model for all tacks in terms of n' and the rate of dissipated pseudo-strain energy is given in the following equations:

$$\frac{\partial \Phi(t)}{\partial t} = \left(10^{-4.227n'-1.231}\right)^{\frac{1}{n'+1}} \left[\frac{1}{2\pi a^2}\frac{\partial W_R}{\partial t}\right]^{\frac{n'}{n'+1}} \tag{36}$$

In future works, the verification and sensitivity analysis of A' and n' would be required. If n' and the rate of dissipated pseudo-strain energy are defined as a function of temperature, loading and debonding rates, and asphalt type, the damage growth could

be predicted at a desired condition. Further investigation on other factors that may affect tackiness would be also needed to improve the damage model.

CHAPTER VI

CONCLUSIONS AND RECOMMENDATIONS[‡]

Trackless tacks play a prominent role in bonding layers under a thin overlay pavement without tracking, which is one of the concerns in using traditional tacks. However, there has been insufficient research on the characterization and performance evaluation of trackless tacks. Thus, the main objectives of this study were to investigate the material characterization of trackless tacks, evaluate the interlayer resistance of trackless tacks, and develop a predictive model for the tracking behavior based on a fundamental fracture theory. The rheological properties of tack residual binders are identified through the DSR frequency sweep and MSCR tests. The surface energy components of the tacks were calculated using the contact angles obtained from the sessile drop test. Also, the tackiness was measured at different temperatures and debonding rates using the DSR tackiness test and quantified in terms of tack energy. Also, the shear bond strength and energy were measured in evaluating the interlayer shear resistance. A variety of factors affecting the interface bonds were also evaluated using laboratory compacted samples and field cores. Based on these test results, the major findings are as follows:

[‡] Part of this chapter is reprinted with permission from "Evaluating Tack Properties of Trackless Tack Coats Through Dynamic Shear Rheometer" by Seo, A.Y., Sakhaeifar, M.S. and Wilson, B.T. (2017) Transportation Research Record: Journal of the Transportation Research Board, 2632(1), 119–129, Copyright 2017 by National Academy of Sciences and "Performance Evaluation and Specification of Trackless Tack" by Wilson, B. T., Seo, A. and Sakhaeifar, M. S. (2016) College Station, TX: Texas A&M Transportation Institute, FHWA/TX-16/0-6814-1, Copyright 2016 by Texas A&M Transportation Institute.

- Using the complex shear modulus obtained from the DSR frequency sweep test, the tack materials are classified into two groups based on their modulus values: control tack, Tack A, B, and C classified in the soft-residue group, and Tack D, and E classified in the stiff-residue group.
- The MSCR test revealed that the percent recovery decreases with increase in stress level for all material types. For the soft-residue group, considerable changes in percent recovery and non-recoverable creep compliance were observed at high stress level conditions. However, the percent recovery and non-recoverable creep compliance of the stiff-residue group did not decrease significantly under this condition.
- The results of adhesion based on surface energy showed that the tack-tire system was more likely to fail at the interface whereas the tack-stainless steel and aggregate systems had a higher occurrence of failure within the tacks. Among the tacks, the control tack showed better wettability on the stainless steel and the rubber than the trackless tacks.
- Through the DSR tackiness test, the tackiness properties of investigated samples cured at different temperatures and curing periods could be evaluated by comparing the changes of tackiness energy and peak force with curing time. Apparent distinctions could be observed between the soft and stiff binder group in regard to their tack energy and failure modes of both emulsion and residue samples.

- In general, a trackless tack having low tack energy (stickiness) measured by the DSR tackiness test with adhesive failure is preferable to be used in construction. Either clean or dirty tip with high tack energy is also acceptable for trackless tacks in the tackiness test. As a result, the stiff binder group had better tracking resistance than the soft binder group.
- The laboratory samples exhibit a high shear bond strength between 689 and 1,379 kPa. Many laboratory samples did not fail at the interface, indicating that the interface bond is stronger than the internal strength of a substrate or overlay layer.
- The bond strength of field cores is noticeably lower than that of laboratory compacted samples. Also, interface failure occurs for all field cores.
- The factors that affect the bonding performance are evaluated through laboratory and field testing as follows:
    a) Tack type: has a remarkable impact on shear resistance at lower tack reactivation temperature. The laboratory samples glued with tack materials in the soft-residue group exhibit lower bond energy than ones in the stiff-residue group due to interface failure. The sensitivity of bond strength to tack type is different for field cores with the existing layer. The field cores applied with the tack in the stiff-residue group exhibits higher shear bond strength regardless of surface type.
    b) Surface type: has a significant effect on shear bond strength and bond energy. The laboratory samples with HMA substrate layer have higher

shear resistance than the ones with concrete substrate. The field samples in the new HMA and milled sections have higher bond strengths than in the existing HMA sections.

c) Compaction angle: marginally affects the bond strength.

d) Reactivation temperature: have a significant impact on shear bond strength and bond energy. The shear bond energy increases with higher reactivation temperature. The tack samples in the stiff-residue group have higher bond energy than the ones in the soft-residue group.

e) Tack rate: due to the limited test results it was found that the shear bond strength was less sensitive to the changes of tack rate compared to the tack and surface types. It should be noted that the limited test results from field samples and the low number of replicates for the tack rate may not be enough to distinguish its impact on interlayer shear resistance.

- Based on the modified Paris's law with the damage density, the fracture properties of tack materials were identified from the results of the tackiness and frequency sweep tests. The tack materials had a good correlation between $-\log A'$ and n'.

In order to produce stronger bonds with tacks, the researchers suggest that overlay mixture be compacted at higher ambient and mix temperatures. Also, the substrate surface condition is an important factor affecting the bond strength. The tack application may not be required to construct the overlay over new HMA as long as the compaction temperatures are high enough. When a thin lift overlay is constructed on

heavily polished pavements, using an underseal having a stiffer residue or milling is recommended to ensure a better bond. Prior to tack application, it is necessary to remove the excessive dirt deposited on the grooves of a milled surface. Based on the available and limited test results in this study an optimum residual tack rate is to use a moderate level (0.14-0.23 L/m^2) in existing and milled layers and a low level (0.05-0.14 L/m^2) in a new layer.

The long-term bonding performance of trackless tacks in the test sections built during this project would be evaluated in future works. It would help set up the criteria that suggest an acceptable bonding performance in field. Also, to fully assess these products, further investigation on the factors influencing tackiness like contact pressure, holding time, and film thickness is needed and being pursued by the research team.

REFERENCES

Ahmad, N., 2011. *Asphalt Mixture Moisture Sensitivity Evaluation Using Surface Energy Parameters.* Dissertation (Doctor of Philosophy). University of Nottingham.

Al-Assi, M. and Kassem, E. 2017. Evaluation of Adhesion and Hysteresis Friction of Rubber–Pavement System. *Applied Sciences*, 7(10), 1029.

Al-Qadi, I. L., *et al.*, 2008. *Tack Coat Optimization for HMA Overlays: Laboratory Testing.* Rantoul, IL: Illinois Center for Transportation, FHWA-ICT-08-023.

Al-Qadi, I. L., *et al.*, 2012. *Best Practices for Implementation of Tack Coat: Part I-Laboratory Study.* Rantoul, IL: Illinois Center for Transportation, FHWA-ICT-12-004.

Amelian, S. and Kim, Y.-R., 2017. *Evaluation of Tack Coating Practices for Asphalt Overlays in Nebraska.* Lincoln, NE: Nebraska Transportation Center, SPR-P1(16) M039.

Anderson, R. M., 2011. *Understanding the MSCR Test and Its Use in the PG Asphalt Binder Specification* [online]. Asphalt Institute. Available from: http://www.asphaltinstitute.org/wp-content/uploads/public/asphalt_academy/webinars/pdfs/MSCR_Webinar_Aug2011.pdf.

Andrews, E. H. and Kinloch, A. J. 1973. Mechanics of Adhesive Failure. I. *Proceedings of the Royal Society of London A: Mathematical, Physical and Engineering Sciences*, 332(1590), 385-399.

Aubrey, D., Welding, G. and Wong, T. 1969. Failure Mechanisms in Peeling of Pressure-Sensitive Adhesive Tape. *Journal of Applied Polymer Science,* 13(10), 2193-2207.

Aymonier, A., *et al.* 2003. Control of Structure and Tack Properties of Acrylic Pressure-Sensitive Adhesives Designed by a Polymerization Process. *Journal of Applied Polymer Science,* 89(10), 2749-2756.

Bae, A., *et al.* 2010. Effects of Temperature on Interface Shear Strength of Emulsified Tack Coats and Its Relationship to Rheological Properties. *Transportation Research Record: Journal of the Transportation Research Board,* (2180), 102-109.

Bahia, H., Jenkins, K. and Hanz, A., Performance Grading of Bitumen Emulsions for Sprayed Seals. ed. *International Sprayed Sealing Conference*, 2008 Adelaide, Australia.

Bhasin, A., *et al.* 2006. Limits on Adhesive Bond Energy for Improved Resistance of Hot-Mix Asphalt to Moisture Damage. *Transportation Research Record: Journal of the Transportation Research Board,* (1970), 3-13.

Bibette, J., Calderon, F. L. and Poulin, P. 1999. Emulsions: Basic Principles. *Reports on Progress in Physics,* 62(6), 969.

Boussad, N. and Martin, T., Emulsifier Content in Water Phase and Particle Size Distribution: Two Key-Parameters for the Management of Bituminous Emulsion Performance. ed. *Eurasphalt and Eurobitume Congress*, 1996 Strasbourg, France.

Boxler, C., Augustin, W. and Scholl, S. 2014. Influence of Surface Modification on the Composition of a Calcium Phosphate-Rich Whey Protein Deposit in a Plate Heat Exchanger. *Dairy Science and Technology*, 94(1), 17-31.

Bueno, H., 2005. *The Critical Surface Tension of 316l Stainless Steel.* Thesis (Master of Science). San Jose State University.

Chen, Y., *et al.* 2012. Effects of Trackless Tack Interface on Pavement Top-Down Cracking Performance. *Procedia - Social and Behavioral Sciences*, 53, 432-439.

Cheng, D., *et al.* 2002. Surface Energy Measurement of Asphalt and Its Application to Predicting Fatigue and Healing in Asphalt Mixtures. *Transportation Research Record*, 1810(1), 44-53.

Cherepanov, G. 1967. The Propagation of Cracks in a Continuous Medium. *Journal of Applied Mathematics and Mechanics*, 31(3), 503-512.

Clark, T. M., Rorrer, T. M. and McGhee, K. K., 2012. *Trackless Tack Coat Materials: A Laboratory Evaluation for Performance Acceptance.* Charlottesville, VA: Virginia Center for Transportation Innovation and Research, VCTIR 12-R14.

Clyne, T. R. and Marasteanu, M. O., 2004. *Inventory of Properties of Minnesota Certified Asphalt Binders.* St. Paul, MN: University of Minnesota, MN/RC-2004-35.

Creton, C. 2003. Pressure-Sensitive Adhesives: an Introductory Course. *MRS Bulletin,* 28(6), 434-439.

Creton, C. and Fabre, P., 2002. Tack. *Adhesion Science and Engineering: The Mechanics of Adhesion.* Elsevier, 535-575.

Crosby, A. J. and Shull, K. R. 1999. Adhesive Failure Analysis of Pressure-Sensitive Adhesives. *Journal of Polymer Science Part B: Polymer Physics,* 37(24), 3455-3472.

Dahlquist, C., 1969. Pressure-Sensitive Adhesives. *In:* Patrick, R. L. ed. *Treatise on Adhesion and Adhesives.* New York: Marcel Dekker, 219-260.

Dowling, N. and Begley, J., 1976. Fatigue Crack Growth During Gross Plasticity and the J-Integral. *Mechanics of Crack Growth.* ASTM International, 82-105.

Gent, A. and Schultz, J. 1972. Effect of Wetting Liquids on the Strength of Adhesion of Viscoelastic Material. *The Journal of Adhesion,* 3(4), 281-294.

Gent, A. N. and Kinloch, A. J. 1971. Adhesion of Viscoelastic Materials to Rigid Substrates. III. Energy Criterion for Failure. *Journal of Polymer Science Part A-2: Polymer Physics,* 9(4), 659-668.

Gorsuch, C., *et al.*, Measuring Surface Tackiness of Modified Asphalt Binders and Emulsion Residues Using a Dynamic Shear Rheometer. ed. *Proceedings of the Fifty-Eighth Annual Conference Of the Canadian Technical Asphalt Association (CTAA),* 2013 Newfoundland and Labrador, 121-138.

Grillet, A. M., Wyatt, N. B. and Gloe, L. M. 2012. Polymer Gel Rheology and Adhesion. *Rheology,* 3, 59-80.

Hakimzadeh, S., *et al.* 2012. Development of Fracture-Energy Based Interface Bond Test for Asphalt Concrete. *Road Materials and Pavement Design,* 13(sup1), 76-87.

Hallab, N. J., *et al.* 2001. Evaluation of Metallic and Polymeric Biomaterial Surface Energy and Surface Roughness Characteristics for Directed Cell Adhesion. *Tissue Engineering,* 7(1), 55-71.

Hanz, A., Arega, Z. and Bahia, H., Advanced Methods for Quantifying Emulsion Setting and Adhesion to Aggregates. ed. *ISAET Symposium,* 2008.

Hanz, A., Arega, Z. and Bahia, H. U., Rheological Evaluation of Emulsion Residues Recovered Using Newly Proposed Evaporative Techniques. ed. *Transportation Research Board 88th Annual Meeting,* 2009.

Hefer, A. W., Bhasin, A. and Little, D. N. 2006. Bitumen Surface Energy Characterization Using a Contact Angle Approach. *Journal of Materials in Civil Engineering,* 18(6), 759-767.

Howson, J., *et al.* 2011. Comprehensive Analysis of Surface Free Energy of Asphalts and Aggregates and the Effects of Changes in pH. *Construction and Building Materials,* 25(5), 2554-2564.

Howson, J., *et al.* 2012. Relationship Between Bond Energy and Total Work of Fracture for Asphalt Binder-Aggregate Systems. *Road Materials and Pavement Design,* 13(sup1), 281-303.

James, A. 2006. Overview of Asphalt Emulsion. *Transportation Research Circular E-C102,* 1-6.

Kadrmas, A., 2012. Testing of Bond Coat Emulsions. *2016 National Pavement Conference.* Nashville, TN.

Kadrmas, A., 2014. Asphalt Emulsion Residue Recovery Update. *Progress Toward Performance-Graded Emulsified Asphalt Specifications.* Washington, D.C.: Transportation Research Board, 8-12.

Khan, A., Redelius, P. and Kringos, N., 2014. *Surface Energy Measurements and Wettability Investigation of Different Minerals and Bitumen for Cold Asphalts.* Raleigh, NC: CRC Press.

Kwok, D. Y. and Neumann, A. W. 1999. Contact Angle Measurement and Contact Angle Interpretation. *Advances in Colloid and Interface Science,* 81(3), 167-249.

Little, D., *et al.*, 2001. *Microdamage Healing in Asphalt and Asphalt Concrete, Volume I: Microdamage and Microdamage Healing, Project Summary Report.* College Station, TX: Texas Transportation Institute.

Little, D. N., Bhasin, A. and Hefer, A., 2006. *Using Surface Energy Measurements to Select Materials for Asphalt Pavement.* Transportation Research Board, NCHRP Project 9-37.

Luo, X., Luo, R. and Lytton, R. L. 2013. Modified Paris's Law to Predict Entire Crack Growth in Asphalt Mixtures. *Transportation Research Record,* 2373(1), 54-62.

Lytton, R. L., *et al.*, 1993. *Development and Validation of Performance Prediction Models and Specifications for Asphalt Binders and Paving Mixes.* Strategic Highway Research Program Washington, DC.

Majidzadeh, K. and Herrin, M., 1967. Strength-Thickness Relations of Solid-Asphalt-Solid Systems. *Engineering Properties of Roofing Systems.* ASTM International.

Marasteanu, M. and Anderson, D., Improved Model for Bitumen Rheological Characterization. ed. *Eurobitume Workshop on Performance Related Properties for Bituminous Binders*, 1999 Brussels, Belgium.

Marasteanu, M. O. and Anderson, D. A. 2000. Establishing Linear Viscoelastic Conditions for Asphalt Binders. *Transportation Research Record: Journal of the Transportation Research Board,* 1728(1), 1-6.

McGhee, K. K. and Clark, T. M., 2009. *Bond Expectations for Milled Surfaces and Typical Tack Coat Materials Used in Virginia.* Charlottesville, VA: Virginia Transportation Research Council, VTRC 09-R21.

Mittal, K. 1976. Adhesion Measurement of Thin Films. *Active and Passive Electronic Components,* 3(1), 21-42.

Mogawer, W., *et al.* 2011. Evaluation of Binder Elastic Recovery on HMA Fatigue Cracking Using Continuum Damage and Overlay Test Based Analyses. *Road Materials and Pavement Design,* 12(2), 345-376.

Mohammad, L., *et al.* 2010. Effects of Pavement Surface Type and Sample Preparation Method on Tack Coat Interface Shear Strength. *Transportation Research Record: Journal of the Transportation Research Board,* (2180), 93-101.

Mohammad, L. N., *et al.*, 2012. *Optimization of Tack Coat for HMA Placement.* Washington, D.C.: National Cooperative Highway Research Program, NCHRP Report 712.

NCAT, 2015. Bonding of Layers is Critical to Good Performance. *Asphalt Technology News.* Auburn, AL National Center for Asphalt Technology (NCAT) at Auburn University, 10-11.

Okamatsu, T., Yasuda, Y. and Ochi, M. 2001. Thermodynamic Work of Adhesion and Peel Adhesion Energy of Dimethoxysilyl-Terminated Polypropylene Oxide/Epoxy Resin System Jointed with Polymeric Substrates. *Journal of Applied Polymer Science,* 80(11), 1920-1930.

Ondarçuhu, T. 1997. Tack of a Polymer Melt: Adhesion Measurements and Fracture Profile Observations. *Journal de Physique II,* 7(12), 1893-1916.

Paris, P. and Erdogan, F. 1963. A Critical Analysis of Crack Propagation Laws. *Journal of Basic Engineering,* 85(4), 528-533.

Park, S. and Kim, Y. 1999. Interconversion Between Relaxation Modulus and Creep Compliance for Viscoelastic Solids. *Journal of Materials in Civil Engineering,* 11(1), 76-82.

Raab, C. and Partl, M. N. 2008. Investigation into a Long-Term Interlayer Bonding of Asphalt Pavements. *Baltic Journal of Road and Bridge Engineering,* 3(2), 65-70.

Redelius, P. and Walter, J. 2006. Bitumen Emulsions. *Surfactant Science Series,* 132, 383-413.

Rice, J. R. 1968. A Path Independent Integral and the Approximate Analysis of Strain Concentration by Notches and Cracks. *Journal of Applied Mechanics,* 35(2), 379-386.

Robertson, R. E., *et al.*, 2001. *Fundamental Properties of Asphalts and Modified Asphalts, Volume I: Interpretive Report.* FHWA-RD-99-212.

Schach, R. and Creton, C. 2008. Adhesion at Interfaces Between Highly Entangled Polymer Melts. *Journal of Rheology,* 52(3), 749-767.

Schapery, R. 1984. Correspondence Principles and a Generalized J-Integral for Large Deformation and Fracture Analysis of Viscoelastic Media. *International Journal of Fracture,* 25(3), 195-223.

Schapery, R. and Park, S. 1999. Methods of Interconversion Between Linear Viscoelastic Material Functions. Part II—An Approximate Analytical Method. *International Journal of Solids and Structures,* 36(11), 1677-1699.

Schapery, R. A. 1975. A Theory of Crack Initiation and Growth in Viscoelastic Media. *International Journal of Fracture,* 11(1), 141-159.

Seo, A., Sakhaeifar, M. and Wilson, B., Tackiness Properties of Non-Tracking Tack Coats. ed. *Proceedings of the 2016 International Conference on Transportation and Development,* 2016 Houston, TX, 740-751.

Seo, A. Y., Sakhaeifar, M. S. and Wilson, B. T., Chemical-Mechanical Interaction of Non-Tracking Tack Coat and Aggregate on Bond Strength. ed. *Airfield and Highway Pavements*, 2015 Miami, FL, 191-202.

Seo, A. Y., Sakhaeifar, M. S. and Wilson, B. T. 2017. Evaluating Tack Properties of Trackless Tack Coats Through Dynamic Shear Rheometer. *Transportation Research Record: Journal of the Transportation Research Board,* (2632), 119-129.

Sharma, P. and Rao, K. H. 2002. Analysis of Different Approaches for Evaluation of Surface Energy of Microbial Cells by Contact Angle Goniometry. *Advances in Colloid and Interface Science,* 98(3), 341-463.

Si, Z., Little, D. and Lytton, R. 2002. Characterization of Microdamage and Healing of Asphalt Concrete Mixtures. *Journal of Materials in Civil Engineering,* 14(6), 461-470.

Song, K., *et al.* 2019. Interaction of Surface Energy Components between Solid and Liquid on Wettability, and Its Application to Textile Anti-Wetting Finish. *Polymers,* 11(3), 498.

Sperling, L. H., 2005. *Introduction to Physical Polymer Science.* John Wiley & Sons.

Takamura, K., *et al.*, Microsurfacing for Preventive Maintenance: Eco-Efficient Strategy. ed. *International Slurry Seal Association Annual Meeting,* 2001 Maui, Hawaii, 5.

Tashman, L., Nam, K. and Papagiannakis, A., 2006. *Evaluation of the Influence of Tack Coat Construction Factors on the Bond Strength Between Pavement Layers.* Pullman, WA: Washington Center for Asphalt Technology, WA-RD 645.1.

Tordjeman, P., Papon, E. and Villenave, J. J. 2000. Tack Properties of Pressure-Sensitive Adhesives. *Journal of Polymer Science Part B: Polymer Physics,* 38(9), 1201-1208.

Tran, N., Willis, R. and Julian, G., 2012. *Refinement of the Bond Strength Procedure and Investigation of a Specification.* Auburn, AL: National Center for Asphalt Technology, NCAT Report 12-04.

Van Oss, C., Chaudhury, M. and Good, R. 1987. Monopolar Surfaces. *Advances in Colloid and Interface Science,* 28, 35-64.

Van Oss, C. J., Chaudhury, M. K. and Good, R. J. 1988. Interfacial Lifshitz-Van Der Waals and Polar Interactions in Macroscopic Systems. *Chemical Reviews,* 88(6), 927-941.

Wagoner, T. B. and Foegeding, E. A. 2018. Surface Energy and Viscoelasticity Influence Caramel Adhesiveness. *Journal of Texture Studies,* 49(2), 219-227.

West, R. C., Zhang, J. and Moore, J., 2005. *Evaluation of Bond Strength Between Pavement Layers.* Auburn, AL: National Center for Asphalt Technology, NCAT Report 05-08.

Weston, J., 2003. *Tech Notes: Issues Related to Tack Coat* [online]. Materials Laboratory, WSDOT. Available from: http://www.wsdot.wa.gov/NR/rdonlyres/DC652B96-0298-45CD-9345-0960BBC3D39D/0/TackCoatTN2007.pdf [Accessed April 17, 2015].

Wilson, B. T., Seo, A. and Sakhaeifar, M. S., 2016. *Performance Evaluation and Specification of Trackless Tack.* College Station, TX: Texas A&M Transportation Institute, FHWA/TX-16/0-6814-1. Available from: http://tti.tamu.edu/documents/0-6814-1.pdf.

Woodward, R. P., 1999. *Contact Angle Measurements Using the Drop Shape Method.* Portsmouth, VA: First Ten Angstroms Inc.

Yi, J., *et al.* 2018. Studies on Surface Energy of Asphalt and Aggregate at Different Scales and Bonding Property of Asphalt–Aggregate System. *Road Materials and Pavement Design,* 19(5), 1102-1125.

Young, T. 1805. An Essay on the Cohesion of Fluids. *Philosophical Transactions of the Royal Society of London,* 95, 65-87.

Yuan, Y. and Lee, T. R., 2013. Contact Angle and Wetting Properties. *Surface Science Techniques.* Springer, 3-34.

Zhao, H., Cao, J. and Zheng, Y. 2017. Investigation of the Interface Bonding between Concrete Slab and Asphalt Overlay. *Road Materials and Pavement Design,* 18(sup3), 109-118.

Zhou, F., *et al.* 2012. Evaluation of Fatigue Tests for Characterizing Asphalt Binders. *Journal of Materials in Civil Engineering,* 25(5), 610-617.

Zisman, W. A. 1963. Influence of Constitution on Adhesion. *Industrial and Engineering Chemistry,* 55(10), 18-38.

Zosel, A. 1989. Adhesive Failure and Deformation Behaviour of Polymers. *The Journal of Adhesion,* 30(1-4), 135-149.

Zosel, A. 1997. The Effect of Bond Formation on the Tack of Polymers. *Journal of Adhesion Science and Technology,* 11(11), 1447-1457.

Zosel, A. 1998. The Effect of Fibrilation on the Tack of Pressure Sensitive Adhesives. *International Journal of Adhesion and Adhesives,* 18(4), 265-271.